PLOS ONE

RESEARCH ARTICLE

Distinct transcriptomic changes in E14.5 mouse skeletal muscle lacking RYR1 or $Ca_v1.1$ converge at E18.5

Dilyana Filipova[1], Margit Henry[2], Tamara Rotshteyn[2], Anna Brunn[3], Mariana Carstov[3], Martina Deckert[3], Jürgen Hescheler[2], Agapios Sachinidis[2], Gabriele Pfitzer[1], Symeon Papadopoulos[1]*

1 Institute of Vegetative Physiology, Center of Physiology and Pathophysiology, University of Cologne, Cologne, Germany, **2** Institute of Neurophysiology and Center for Molecular Medicine Cologne (CMMC), University of Cologne, Cologne, Germany, **3** Department of Neuropathology, University of Cologne, Cologne, Germany

* spapadop@uni-koeln.de

Citation: Filipova D, Henry M, Rotshteyn T, Brunn A, Carstov M, Deckert M, et al. (2018) Distinct transcriptomic changes in E14.5 mouse skeletal muscle lacking RYR1 or $Ca_v1.1$ converge at E18.5. PLoS ONE 13(3): e0194428. https://doi.org/10.1371/journal.pone.0194428

Editor: Agustín Guerrero-Hernandez, Cinvestav-IPN, MEXICO

Received: January 9, 2018

Accepted: March 4, 2018

Published: March 15, 2018

Data Availability Statement: All microarray data described in this study are available in the ArrayExpress database (www.ebi.ac.uk/arrayexpress) under the accession number E-MTAB-5755.

Funding: This work was supported by grant number KF225/2016 from Köln Fortune (http://medfak.uni-koeln.de/19728.html?&L=1). The funders had no role in study design, data collection and analysis, decision to publish, or preparation of the manuscript.

Abstract

In skeletal muscle the coordinated actions of two mechanically coupled Ca^{2+} channels—the 1,4-dihydropyridine receptor ($Ca_v1.1$) and the type 1 ryanodine receptor (RYR1)–underlie the molecular mechanism of rapid cytosolic [Ca^{2+}] increase leading to contraction. While both $[Ca^{2+}]_i$ and contractile activity have been implicated in the regulation of myogenesis, less is known about potential specific roles of $Ca_v1.1$ and RYR1 in skeletal muscle development. In this study, we analyzed the histology and the transcriptomic changes occurring at E14.5 –the end of primary myogenesis and around the onset of intrauterine limb movement, and at E18.5 –the end of secondary myogenesis, in WT, $RYR1^{-/-}$, and $Ca_v1.1^{-/-}$ murine limb skeletal muscle. At E14.5 the muscle histology of both mutants exhibited initial alterations, which became much more severe at E18.5. Immunohistological analysis also revealed higher levels of activated caspase-3 in the $Ca_v1.1^{-/-}$ muscles at E14.5, indicating an increase in apoptosis. With WT littermates as controls, microarray analyses identified 61 and 97 differentially regulated genes (DEGs) at E14.5, and 493 and 1047 DEGs at E18.5, in $RYR1^{-/-}$ and $Ca_v1.1^{-/-}$ samples, respectively. Gene enrichment analysis detected no overlap in the affected biological processes and pathways in the two mutants at E14.5, whereas at E18.5 there was a significant overlap of DEGs in both mutants, affecting predominantly processes linked to muscle contraction. Moreover, the E18.5 vs. E14.5 comparison revealed multiple genotype-specific DEGs involved in contraction, cell cycle and miRNA-mediated signaling in WT, neuronal and bone development in $RYR1^{-/-}$, and lipid metabolism in $Ca_v1.1^{-/-}$ samples. Taken together, our study reveals discrete changes in the global transcriptome occurring in limb skeletal muscle from E14.5 to E18.5 in WT, $RYR1^{-/-}$ and $Ca_v1.1^{-/-}$ mice. Our results suggest distinct functional roles for RYR1 and $Ca_v1.1$ in skeletal primary and secondary myogenesis.

Competing interests: The authors have declared that no competing interests exist.

Introduction

Skeletal muscle is the largest organ in the vertebrate body. Although the most prominent association coming into mind when one thinks of skeletal muscle is probably that related to contraction and movement, the functional repertoire of this organ is by far more versatile. For instance, involvement in energy metabolism, myokine secretion and further mechanisms of crosstalk with various organs are additional important roles of skeletal muscle [1,2]. Muscle tissue itself shows a high degree of heterogeneity and additional cell types like neurons, smooth muscle and blood cells, as well as fibroblasts and connective tissue contribute to the overall structural and functional characteristics of a certain muscle [3]. Accordingly, the proper formation of the skeletal muscle organ is a complex, only partially understood multistep process, subjected to a strict spatiotemporal regulation throughout development [4].

In mice the formation of skeletal muscle begins around embryonic day E8.5 / E9, when somites differentiate into the sclerotome and dermomyotome, and proceeds until birth (E18.5 –E19) with a subsequent postnatal maturation for 2–3 weeks [5]. Prenatally, skeletal muscle development can be divided into embryonic (from E8.5 until E14.5) and fetal (E14.5 to E18.5 / birth). During the embryonic phase initial myogenic events give rise to the primary myotome and myogenic precursor cells, the latter differentiating into embryonic myoblasts that invade the myotome and fuse into myotubes. Simultaneously, myogenic progenitors migrate from the dermomyotome to the limbs and differentiate into primary multinucleated fibers in a process described as primary myogenesis [6]. In the fetal phase, secondary myogenesis takes place whereby fetal myoblasts, derived from Pax3/Pax7 positive muscle progenitor cells, merge with each other or with primary fibers to form secondary muscle fibers [7,8]. Thus, the primary myogenesis lays the foundation of the developing skeletal muscle and during the secondary myogenesis the muscle grows and differentiates. In line with this notion, a genome wide expression analysis has shown that embryonic and fetal myoblasts have distinct transcriptomic profiles [9]. The proper transition between the different stages in myogenesis is regulated by the strict spatiotemporal expression of canonical myogenic regulatory factors (MRFs) [10] and involves a crosstalk with the surrounding connective and neuronal tissue [4]. Around the time of late embryonic and early fetal development the first skeletal muscle contractions effective in limb movement start appearing in mouse [11].

In skeletal muscle contractions are initiated by action potentials originating from the motor neurons that induce a depolarization wave travelling along deep invaginations of the sarcolemma—the T tubuli. The signal is then transmitted to the sarcoplasmic reticulum (SR)–the major Ca^{2+} reservoir in skeletal muscle, leading to a rapid local Ca^{2+} release from the SR and a high increase of the cytosolic Ca^{2+} concentration $[Ca^{2+}]_i$, which enables muscle contraction—a process known as excitation-contraction coupling (ECC) [12,13]. The released Ca^{2+} participates in a wide variety of signaling pathways and during development is involved in myoblast migration and fusion, as well as in muscle terminal differentiation and growth [14,15]. Additionally muscle contraction, by means of mechanotransduction, triggers downstream cascades which temporary overlap with Ca^{2+}-induced signaling responses and which play a crucial role in skeletal muscle's development and adaptation to exercise [16].

On a molecular level ECC in skeletal muscle can be described as conformational signal transmission between two functionally and, most likely, also mechanically coupled Ca^{2+} channels, the sarcolemmal / t-tubular, voltage-gated $Ca_v1.1$ (also known as 1,4-dihydropyridine receptor, DHPR)and the Ca^{2+} release channel ryanodine receptor type 1 (RYR1), anchored in the SR membrane. $Ca_v1.1$ acts as a voltage sensor who upon membrane depolarization imposes conformational changes on RYR1, causing the latter to release Ca^{2+} from the SR into the sarcoplasm [17]. In the context of ECC the structural, electrophysiological and biochemical

characteristics of both $Ca_v1.1$ and RYR1 have been the subject of numerous investigations [17–21]. Mutations in these channels have been linked to the pharmacogenetic condition of malignant hyperthermia, to hypokalemic periodic paralysis, and to a spectrum of myopathies [22]. The often prenatal onset of the latter [23] implies important functions of the two Ca^{2+} channels in myogenesis.

Two mouse models have been utilized for studying the functions of RYR1 and DHPR—the *dyspedic* mouse, a RYR1 null mutant model ($RYR1^{-/-}$) [24]; and the *dysgenic* mouse—a null mutant for the principal voltage-sensor-containing subunit of the DHPR—$Ca_v1.1$ ($Ca_v1.1^{-/-}$) [25]. While both heterozygous $RYR1^{+/-}$ and $Ca_v1.1^{+/-}$ mutants are allegedly indistinguishable from their WT littermates, the homozygous $RYR1^{-/-}$ and $Ca_v1.1^{-/-}$ mutants cannot support ECC and die at birth from asphyxia [24,26,27]. We have previously shown that at E18.5 the $RYR1^{-/-}$ fetuses exhibit extensive changes in limb skeletal muscle gene expression, affecting major signaling pathways like the mitogen-activated protein kinase (MAPK), Wnt and PI3K-AKT pathways, as well as multiple genes related to muscle structure and function [28]. The wide spectrum of gene expression alterations associated with the complete absence of RYR1 in deed suggested a critical role of this channel in myogenesis. However, the relatively late stage (E18.5) at which we performed the expression analysis probably represented not only expression changes directly related to RYR1 absence, but most likely also comprised a reactive and/or degenerative component.

Here, we examined how the absence of RYR1 or $Ca_v1.1$ affects primary and secondary myogenesis at E14.5 and E18.5, respectively. For both stages we compare the body gross morphology as well the structural features of WT ($RYR1^{+/+}$ and $Ca_v1.1^{+/+}$), heterozygous ($RYR1^{+/-}$ and $Ca_v1.1^{+/-}$) and homozygous ($RYR1^{-/-}$ and $Ca_v1.1^{-/-}$) limb skeletal muscle from littermates. Muscle development was mildly delayed in $RYR1^{-/-}$, $Ca_v1.1^{+/-}$ and $Ca_v1.1^{-/-}$ fetuses at E14.5 as indicated by the higher degree of fascicular disorganization in these animals. Much more severe changes were observed at E18.5, at which stage the limb skeletal muscle of $RYR1^{-/-}$ and $Ca_v1.1^{-/-}$ fetuses consisted almost exclusively of undifferentiated myotubes and amorphous tissue. Structural disorganization was also observed in $Ca_v1.1^{+/-}$ skeletal muscle at E18.5. Expression analysis of MRFs revealed lower mRNA levels for *Six1* in $RYR1^{-/-}$ and for *Mrf4* in $Ca_v1.1^{-/-}$ at E14.5 and of *Pax3* in $RYR1^{-/-}$ at E18.5. At E14.5 $RYR1^{-/-}$ skeletal muscle exhibited high expression levels of an embryonic $Ca_v1.1$ splice variant, Δ29, indicating that the presence of RYR1 impacts the advancement of the myogenic schedule.

We performed microarray analyses (MAs) using RNA isolated from limb skeletal muscle at E14.5 or E18.5 to characterize the transcriptome of $RYR1^{-/-}$ and $Ca_v1.1^{-/-}$ mice versus their respective WT littermates. While we find almost no overlap in the transcriptomic changes (compared to WT) of $RYR1^{-/-}$ and $Ca_v1.1^{-/-}$ samples at E14.5, at E18.5 we reveal a significant convergence of differential gene expression in both mutants, with common DEGs primarily associated with muscle contraction. However, our analysis also reveals processes and structures which are affected in a mutant-specific manner, e.g., the extracellular matrix (ECM) in $RYR1^{-/-}$ and lipid metabolism in $Ca_v1.1^{-/-}$ skeletal muscle. Finally, we find further indications that both mutants recapitulate only the incomplete myogenic program as the amount of DEGs, microRNAs and regulated processes, when going from E14.5 to E18.5, is by far greater in samples from WT skeletal muscle.

Materials and methods

Ethics statement

Animal experiments were carried out in accordance with the guidelines of the European Commission (Directive 2010/63/EU) and of the German animal welfare act (TierSchG). The mice

were housed in the Animal Facility of the Center for Molecular Medicine Cologne (CMMC), a part of the Medical Faculty of the University of Cologne according to the European Union Recommendation 2007/526/EG. All experimental protocols were approved by the local governmental authorities (Landesamt für Natur, Umwelt und Verbraucherschutz, North Rhine-Westphalia, 84–02.04.2015.A054). Effort was taken to minimize animal suffering.

Animals and skeletal muscle preparation

Both the $RYR1^{+/-}$ *dyspedic* ($ry1_{42}$) and the $Ca_v1.1^{+/-}$ *dysgenic* mouse (*mdg*) lines, were from the C57BL/6J background [27,29]. Six heterozygous $RYR1^{+/-}$ or $Ca_v1.1^{+/-}$ male and female mice were subjected to timed mating (pairing was only among lines: either $RYR1^{+/-}$ x $RYR1^{+/-}$ or $Ca_v1.1^{+/-}$ x $Ca_v1.1^{+/-}$). Three pregnant females of each line were sacrificed at day 14.5 and three at day 18.5 post coitum by cervical dislocation and each fetus was prepared and handled separately [28]. Skeletal muscle from the front and hind limbs of each fetus was dissected as previously described [28], pooled for each animal in RNAlater (Cat. No. 76104, Qiagen, Hilden, Germany) on ice during sample collection and centrifuged for 10 min at 16,000 x g. The RNAlater was then removed and the samples were immediately frozen in liquid nitrogen and stored at -80 ˚C until use.

The fetuses were genotyped via PCR as described below. From each litter the limb skeletal muscle samples from one WT, one heterozygous (either $RYR1^{+/-}$ or $Ca_v1.1^{+/-}$) and one homozygous (either $RYR1^{-/-}$ or $Ca_v1.1^{-/-}$) mutant littermate were used in the subsequent analyses (n = 3 biological replicates = 3 animals for each group).

Genotyping

A small terminal segment from the tail of each fetus was lysed in 100 μl lysis buffer (25 mM NaOH, 0.1 mM EDTA) at 95 ˚C for 30 minutes, followed by an addition of 100 μl ice-cold neutralization buffer (40 mM Trizma-HCl) on ice. One μl of each sample was used as a template for genotyping PCRs using the DreamTaq Polymerase (Thermo Scientific, Cat. #EP0703) as per manufacturer's instructions. For genotyping the RYR1 line *(Ryr1* gene), primers forward: 5′- GGACTGGCAAGAGGACCGGAGC -3′ and reverse: 5′-GGAAGCCAGGGCTGCAGGTG AGC-3′ were used for detection of the WT (+) allele; and primers forward: 5'-GGACTGGCAA GAGGACCGGAGC -3′ and reverse: 5′-CCTGAAGAACGAGATCAGCAGCCTCTGTCCC-3′- for the detection of the mutant (-) allele. Primers forward: 5′-GCTTTGCAGATGTTCGGGAA GATCGCCATGG-3′ and reverse: 5′-GCAGCTTTCCACTCAGGAGGGATCCAGTGT-3′ were used for genotyping the $Ca_v1.1$ line (*Cacna1s* gene), the resulting PCR products being subsequently subjected to a restriction analyses via *Ear*I (NEB, Cat. #R0528S). *Ear*I digests only the PCR product from the WT *$Ca_v1.1$* allele but not the mutant allele. PCR products and *Ear*I digestions were analyzed via runs on 2% agarose gels.

Morphological analyses

Comparison of the overall morphology, body shape and size of littermates from different genotypes, was carried out after taking whole-body photographs of animal fetuses (n = 3) at E14.5 and E18.5 of each of the following genotypes: $RYR1^{+/+}$ (WT), $RYR1^{+/-}$, $RYR1^{-/-}$; $Ca_v1.1^{+/+}$ (WT), $Ca_v1.1^{+/-}$, and $Ca_v1.1^{-/-}$. Representative photographs from each group are shown.

Histology and immunohistochemistry

The entire hind limbs of E14.5 and E18.5 fetuses were prepared and mounted on thick filter paper with Tissue-Tek OCT compound (Miles Scientific, Naperville, IL), snap-frozen in isopentane (Fluka, Neu-Ulm, Germany) pre-cooled by dry ice, and stored at −80˚C until

preparation of serial 10 μm frozen sections. Sections were stained with H&E. Immunohistochemistry to detect apoptosis was performed with monoclonal rabbit anti-mouse activated caspase-3 (clone C92-605; BD Biosciences, Heidelberg, Germany) by use of the avidin-biotin complex technique with appropriate biotinylated secondary antibodies (Vectastain Elite Kit; Vector Laboratories, Burlingame, CA). Peroxidase reaction product was visualized using 3,3'-diaminobenzidine (Sigma-Aldrich) as chromogene and H_2O_2 as co-substrate.

RNA extraction

Total skeletal muscle RNA was extracted from limb skeletal muscles as described previously [28]. Briefly, the muscle tissue was rapidly homogenized mechanically via a steel micropestle (Cat. #6–1062, neoLab, Heidelberg, Germany) in liquid nitrogen. Total RNA was extracted with the *Maxwell 16 LEV simplyRNA Tissue Kit* (Cat. #AS1280, Promega, Madison, WI) using a Maxwell 16 instrument (Cat. #AS2000, Promega, Madison, WI) according to the manufacturer's instructions. RNA concentration was measured with a NanoDrop 1000 Spectrophotometer (Peqlab, Erlangen, Germany). 250 or 500 ng of each RNA sample were analyzed via runs on 2% agarose gels next to 2 μl of RiboRuler High Range RNA Ladder (Cat. # SM1821, ThermoFisher Scientific, Hagen, Germany).

cDNA synthesis and quantitative real-time PCRs (qRT-PCRs)

1 μg total RNA of each sample was used for cDNA synthesis via the QuantiTect® Reverse Transcription Kit (Cat. #205311 Qiagen, Hilden, Germany) according to the manufacturer's instructions. Samples were eluted in a final volume of 500 μl nuclease-free water. qRT-PCR analyses were applied for determination of the relative gene expression levels of selected genes as previously described [28]. All primers (Table 1) were designed using the Primer-BLAST[30] online tool (NCBI, www.ncbi.nlm.nih.gov/tools/primer-blast/) with a Tm range of 58 ˚C–60 ˚C, an optimal length of 20 bases and an amplicon of 105–115 bp, and were purchased from Sigma Aldrich (Munich, Germany). The qRT-PCR reaction mixtures were prepared via the GoTaq® qPCR Master Mix kit (Cat. #A6001, Promega, Madison, WI) and relative expression levels were calculated as fold change (FC) using the $2^{-\Delta\Delta Ct}$ method as previously described [28] with the *Cytb* transcript as endogenous control.

Microarrays

All microarray reagents, including the 36 Gene-Chips, and the instrumentation used for the microarray analyses were from Affymetrix (ThermoFischer Scientific Waltham, MA, USA). 250 ng total RNA were used for reverse transcription and the resulting cDNA was fragmented and labeled via the GeneChip® WT PLUS Reagent Kit as per the manufacturer's instructions (Affymetrix). The labeled cDNA samples were hybridized to Affymetrix MoGene 2.0 ST arrays and incubated in Genechip Hybridization Oven-645 (Affymetrix) rotating at 60 rpm at 45˚C for 16 h. Subsequently, arrays were washed on a Genechip Fluidics Station-450 (Affymetrix) and stained with the Affymetrix HWS kit according to the manufacturer's protocol. Finally, the chips were scanned with an Affymetrix Gene-Chip Scanner-3000-7G and the Affymetrix GCOS software was used for the generation of .dat and .cel files. Microarray data are available in the ArrayExpress database (www.ebi.ac.uk/arrayexpress) under the accession number E-MTAB-5755.

Statistical analysis

The .cel files obtained by the microarray analyses were subjected to background correction, summarization and normalization by Robust Multiarray Analysis (RMA) and used for

Table 1. Primers sequences and amplicon size used in qRT-PCR analyses.

Gene	Primers (5' to 3')	Amplicon (bp)
Abra	Fwd: GCCCCCAAAACTCTGTCTCC	111
	Rev: GACAACCGTTCTGGTCACCT	
Actb	Fwd: GCCTCACTGTCCACCTTCCA	115
	Rev: AAAACGCAGCTCAGTAACAGTC	
Ankrd1	Fwd: CCTGCGAGGCTGATCTCAAT	110
	Rev: CGCACCGAAGGTCATCAAGA	
Cacna1s exons 10–11	Fwd: GCCACTCTGGTTGACCCATT	115
	Rev: GGACATGAAGTACTGGCGCA	
Cdh3	Fwd: CAACGAAGCCCCTGTGTTTG	109
	Rev: CTCCTTGTCTGGGTCCTGTG	
Col19a1	Fwd: TTGGATTGCCAGGAGAACAT	114
	Rev: CAGCATCACCCTTCAGACCT	
Creb5	Fwd: AGGGAGTTGAAGGCTACTGGA	107
	Rev: TCTGCAGCTCCGACCTATCT	
Cytb	Fwd: CCATTCTACGCTCAATCCCCA	109
	Rev: AGGCTTCGTTGCTTTGAGGT	
Derl3	Fwd: ATGCTCTTCGTGTTCCGCTA	109
	Rev: GCAGAGTCATAAGAACACCACC	
Eda2r	Fwd: AGAGGATGGATTTGATCTGTTGTTG	106
	Rev: AAGGCAGTTGTCACGCTCTC	
Fn1	Fwd: GGTTCGGGAAGAGGTTGTGA	105
	Rev: ATGGCGTAATGGGAAACCGT	
Fos	Fwd: AGTCAAGGCCTGGTCTGTGT	100
	Rev: TCCAGCACCAGGTTAATTCC	
Gapdh	Fwd: AGTGTTTCCTCGTCCCGTAG	119
	Rev: TGATGGCAACAATCTCCACT	
Hbb-y	Fwd: TTGGCTAGTCACTTCGGCAAT	107
	Rev: AGGGCTCAGTGGTACTTGTG	
Hdac4	Fwd: CCAATGCCAATGCTGTCCAC	112
	Rev: TGCGCCTCAATCAGAGAGTG	
Irx2	Fwd: GTCTACACGTCGACTCGCTC	107
	Rev: ACACTCTGAGCCTGATTCGC	
Klf4	Fwd: TACCCCTACACTGAGTCCCG	110
	Rev: GGAAAGGAGGGTAGTTGGGC	
Mcpt4	Fwd: GTGGGCAGTCCCAGAAAGAA	107
	Rev: GCATCTCCGCGTCCATAAGA	
Mlip	Fwd: AAGCATGAACCAGGAAGCTCA	114
	Rev: CTGGACCCTCTCTTGTTTGCT	
Mrf4	Fwd: GCAGAGGGCTCTCCTTTGTA	105
	Rev: AACGTGTTCCTCTCCACTGC	
Mybpc2	Fwd: ACACTGAACATCCGCCGAC	113
	Rev: TGTGGCACTCGGACATCCA	
Myf5	Fwd: GAAGGTCAACCAAGCTTTCG	109
	Rev: GCTCTCAATGTAGCGGATGG	
Myl2	Fwd: AAAGAGGCTCCAGGTCCAAT	105
	Rev: CACCTTGAATGCGTTGAGAA	

(*Continued*)

Table 1. (Continued)

Gene	Primers (5' to 3')	Amplicon (bp)
Mylpf	Fwd: ATAACCCCAGAAGAACTGCTCC	108
	Rev: TTCTCTTGGCCTTCTTGGGTG	
Myod	Fwd: GGCTACGACACCGCCTACTA	110
	Rev: GTGGAGATGCGCTCCACTAT	
Myog	Fwd: CTGCACTCCCTTACGTCCAT	103
	Rev: CCCAGCCTGACAGACAATCT	
Nefl	Fwd: TTCAGGATCTATGGCAATGTGA	115
	Rev: TCCCATGAGGTTGCACATGAA	
Nell1	Fwd: ATCAGAGGAAGGCGTTTGGG	111
	Rev: AGCACGGAGACTCAACAACC	
Pax3	Fwd: AAACCCAAGCAGGTGACAAC	115
	Rev: AGACAGCGTCCTTGAGCAAT	
Pax7	Fwd: ATTACCTGGCCAAAAACGTG	105
	Rev: AGTAGGCTTGTCCCGTTTCC	
Rplp0	Fwd: GATTCGGGATATGCTGTTGG	108
	Rev: TCGGGTCCTAGACCAGTGTT	
Six1	Fwd: CCTGGGGCAAAATGATGTAT	112
	Rev: CAAAGCATGAGCAAGCCAAC	
Six4	Fwd: GGCCAGAGGTTGTTGTTTGT	109
	Rev: GGCAGCCAAGCTGTGTAAGT	
Sox10	Fwd: TACCTTTGCCTTGCACCCTT	111
	Rev: AAAGGGGCAGCGATGTGTTA	
Trpm3	Fwd: AAGGCTTTGACTTTCTGTCATCTG	105
	Rev: TTCAACAGTGGGTCCAATAGCA	
Uba52	Fwd: ATTGAGCCATCCCTTCGTCAG	111
	Rev: CTTCTTCTTGCGGCAGTTGAC	
Ucp1	Fwd: GGAGGTGTGGCAGTGTTCAT	112
	Rev: AAGCATTGTAGGTCCCCGTG	

https://doi.org/10.1371/journal.pone.0194428.t001

generation of .chp summarization files via the Expression Console™ Software 1.4 (Affymetrix), and subsequently were used to produce a three dimensional PCA plot. The .chp files were used for gene level differential expression quantification, accompanied by One-Way Between-Subject ANOVA statistical analysis via the Transcriptome Analysis Console 3.0 (Affymetrix). Transcripts having a p-value ≤ 0.05 and a linear FC $\geq \pm 2$ for comparison of E18.5 vs. E14.5 sample groups, or a FC $\geq \pm 1.5$ for E14.5 vs. E14.5 and E18.5 vs. E18.5 sample groups, were considered as differentially expressed genes (DEGs). Volcano plots were generated using the Transcriptome Analysis Console 3.0 (Affymetrix).

GraphPad Prism version 4.00 (GraphPad Software, La Jolla California USA, www.graphpad.com) was utilized for the statistical analysis of all qRT-PCR data. Unpaired t-test analyses were done when comparing the relative expression levels of one test group versus one control and one-way ANOVA followed by Bonferroni's multiple comparisons test was performed when comparing multiple groups.

Enrichment analyses

Gene enrichment analyses for DEGs identified upon the comparisons of different groups were performed with the databases *Gene Ontology for Biological Process* (GO BP) and *Cellular*

Component (GO CC), as well as with *Wiki Pathways* (WP) using the *Enrichr* online enrichment tool [31]. A p-value ranking was applied to all enrichment analyses.

Heatmaps and hierarchical clustering

Heatmaps and hierarchical clustering analyses were performed via the *ClustVis* online tool [32] using unit variance row scaling. Hierarchical average linkage clustering measuring the average Euclidean distance was applied for both rows and columns.

Analysis of $Ca_v1.1$ full length and Δ29 splice variants

To determine, within the same sample, the relative amount of $Ca_v1.1$ transcripts containing or missing exon 29, i.e. $Ca_v1.1$ full length and Δ29 respectively, the cDNA produced from 10 ng total RNA from each sample was used as template for PCR analysis. The region between $Ca_v1.1$ exons 28 and 30 was amplified using the forward primer `5′-TCCTAATCGTCATCGGCAGC-3′` and the reverse primer `5′-TTTATCTGCGTCCCGTCCAC-3′`. PCRs were performed using the DreamTaq Polymerase (Cat. #EP0703, ThermoFisher Scientific, Hagen, Germany) according to the manufacturer's protocol. The PCR program consisted of an initial DNA denaturing step at 95˚C for 3 minutes, followed by 35 cycles of 95˚C for 30 seconds, 55˚C for 30 seconds and 72˚C for 1 minute; with a subsequent 5 minute elongation step at 72˚C and a final holding step at 4˚C. Transcripts containing exon 29 produced a 343 bp PCR product while those lacking exon29 resulted in a smaller product, 286 bp. The two PCR products were separated electrophoretically on 2% agarose gels and the bands were digitized via the INTAS documentation system (version 3.28.16.01.2009). Band intensities were quantified with the image analysis module implemented in the FluoView1000 software (Olympus, Japan). In the process of band intensity quantification, background correction was performed locally for each lane. Subsequently, the intensity integral of each band was calculated by summing the intensity values of all pixels belonging to that band. The sum of the two intensity integrals was regarded as 100%, so that the fractional intensity (in %) of each band, with or without exon 29, could be calculated.

Results

Altered gross morphology of $RYR1^{-/-}$ and $Ca_v1.1^{-/-}$ fetuses at E18.5 but not at E14.5

First, we examined the effects of the absence of either RYR1 or $Ca_v1.1$ on the gross morphological appearance at embryonic days E14.5 and E18.5. For this assessment 3 littermates from each genotype, $RYR1^{+/+}$ (WT), $RYR1^{+/-}$ and $RYR1^{-/-}$, as well as $Ca_v1.1^{+/+}$ (WT), $Ca_v1.1^{+/-}$ and $Ca_v1.1^{-/-}$, at both E14.5 and E18.5, were used for whole embryos preparations (Fig 1). At E14.5 no apparent macroscopic differences in the morphology were observed between the WT, heterozygous ($^{+/-}$) and homozygous ($^{-/-}$) mutants of either mouse line. For the E18.5 stage, it was already known from previous studies that homozygous $RYR1^{-/-}$ and $Ca_v1.1^{-/-}$ mutants, in comparison to their WT littermates, exhibit clear morphological alterations comprising a characteristic spinal curvature, smaller limbs and enlarged necks, as well as a smaller body size [24,27]. Our own observations on E18.5 mice confirm these findings, but show additionally that there is no distinguishable gross morphology between $RYR1^{+/-}$ or $Ca_v1.1^{+/-}$ heterozygous fetuses compared to their WT littermates at this later stage (Fig 1).

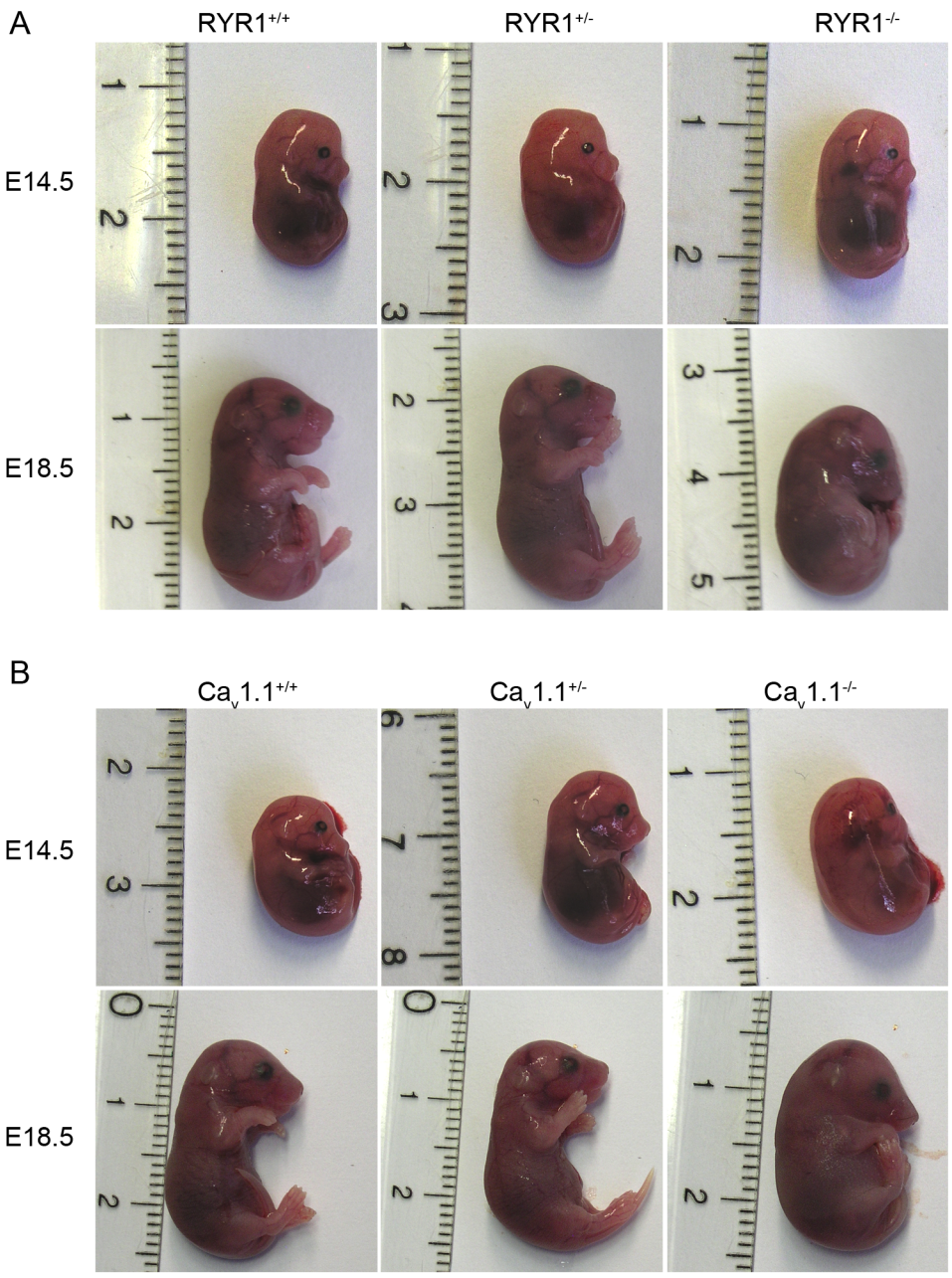

Fig 1. Gross fetal morphology at E14.5 and E18.5. Photographs of whole fetuses were obtained at E14.5 and E18.5 for $RYR1^{+/+}$ (WT), $RYR1^{+/-}$ and $RYR1^{-/-}$ littermates (A), as well as for $Ca_v1.1^{+/+}$ (WT), $Ca_v1.1^{+/-}$ and $Ca_v1.1^{-/-}$ littermates (B).

https://doi.org/10.1371/journal.pone.0194428.g001

Altered morphology of homozygous, $RYR1^{-/-}$ and $Ca_v1.1^{-/-}$, but also of heterozygous $Ca_v1.1^{+/-}$ fetuses at E14.5 and E18.5

Next, we analyzed serial cross sections from the hind limbs of WT, heterozygous ($^{+/-}$), and homozygous ($^{-/-}$) RYR1 and $Ca_v1.1$ mice at E14.5 (Fig 2) and E18.5 (Fig 3). At E14.5 WT muscles consisted predominantly of myotubes; some primary muscle fibers were already detectable and fascicle formation was already initiated (Fig 2A and 2B). While the morphology

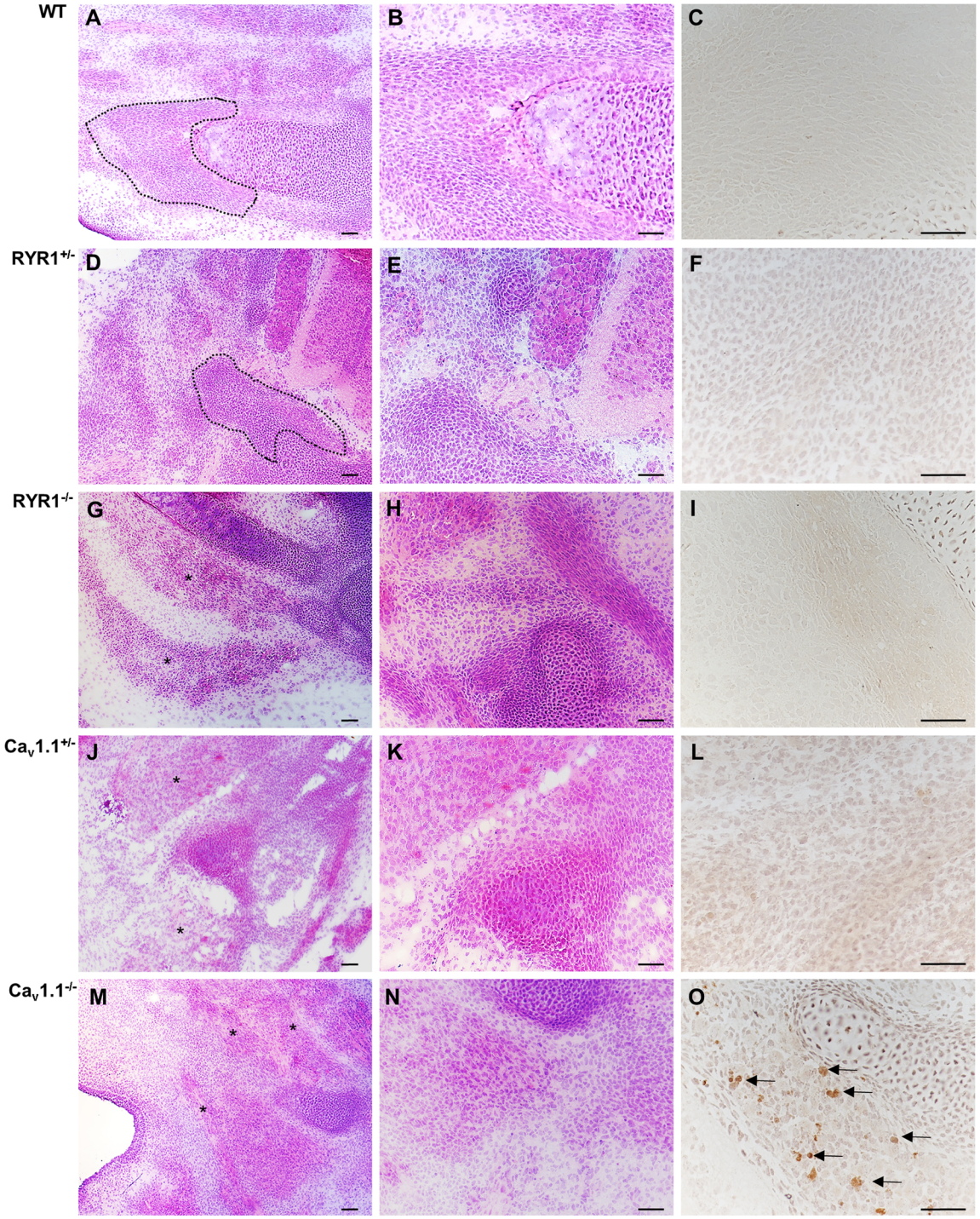

Fig 2. Histology of mouse limb skeletal muscle at embryonic day E14.5. Cross sections of the lower hind limb of a WT fetus (A-C), a $RYR1^{+/-}$ fetus (D-F), a $RYR1^{-/-}$ fetus (G-I), a $Ca_v1.1^{+/-}$ fetus (J-L), and a $Ca_v1.1^{-/-}$ fetus (M-O), respectively. At E14.5, the skeletal muscle of the hind limb of a WT fetus (A, B) as well as of a $RYR1^{+/-}$ fetus (D, E) already harbor muscle fascicles (surrounded by dotted line) consisting of numerous muscle fibers while myoblasts were virtually absent. In contrast, the skeletal muscle of the hind limb of a $RYR1^{-/-}$ (G, H), a $Ca_v1.1^{+/-}$ (J, K), and a $Ca_v1.1^{-/-}$ (M, N) fetus, respectively, exhibits disorganization (asterisks) or complete absence of muscle fascicles and numerous myoblasts. Immunohistochemistry with anti-activated caspase-3 reveals prominent apoptosis only in nuclei of the myotubes of a $Ca_v1.1^{-/-}$ fetus at E14.5 (O, arrows). H&E staining (A, B, D, E, G, H, J, K, M, and N); original magnification x100 (A, D, G, J, M) and x200 (B, E, H, K, N). Immunohistochemistry with rabbit anti-mouse activated caspase-3 (clone C92-605; BD Biosciences) and slight counterstaining with hemalum; original magnification x400. Scale bars correspond to 100 μm in all microphotographs.

https://doi.org/10.1371/journal.pone.0194428.g002

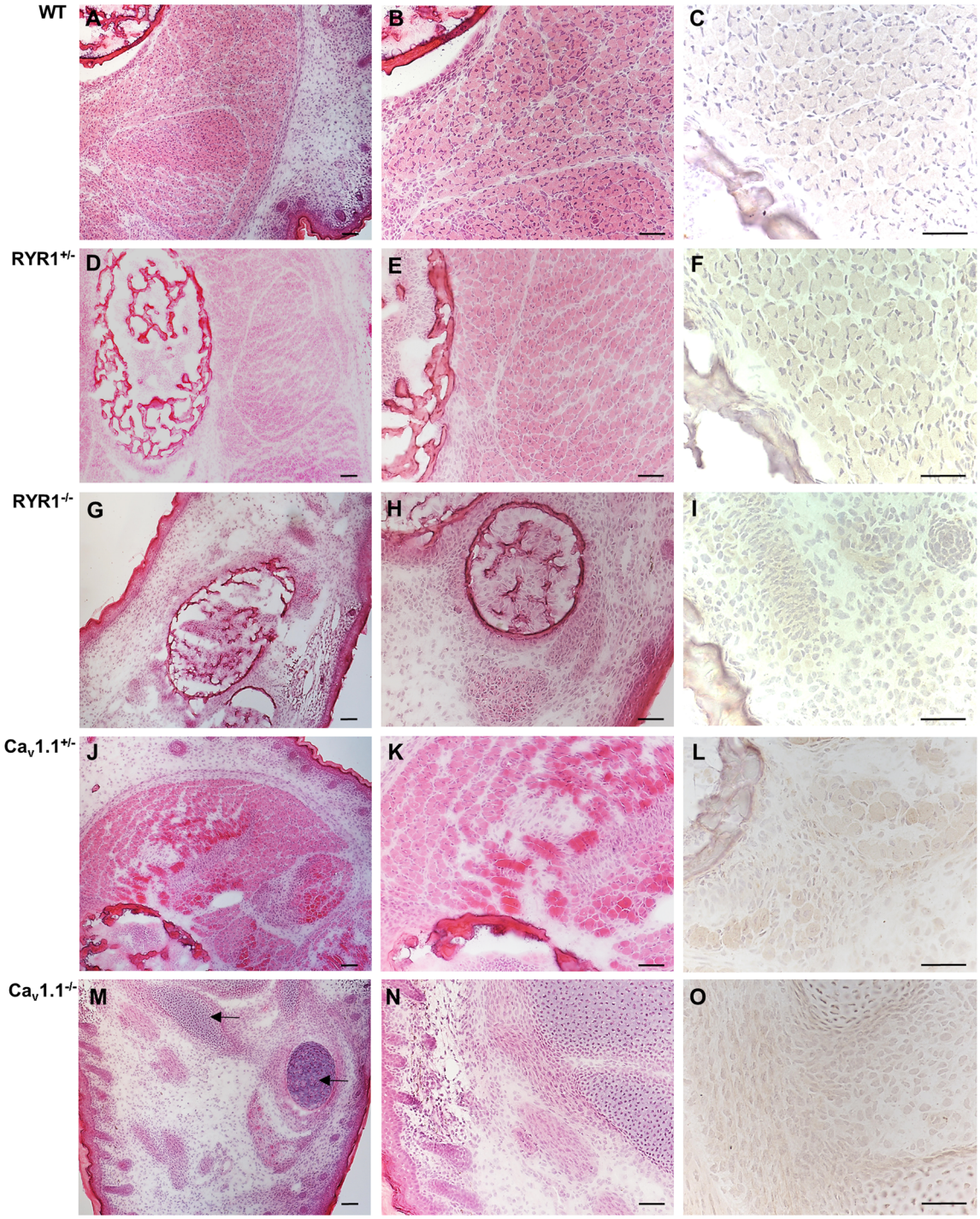

Fig 3. Histology of mouse limb skeletal muscle at embryonic day E18.5. Cross sections of the lower hind limb of a WT fetus (A-C), a $RYR1^{+/-}$ fetus (D-F), a $RYR1^{-/-}$ fetus (G-I), a $Ca_v1.1^{+/-}$ fetus (J-L), and a $Ca_v1.1^{-/-}$ fetus (M-O), respectively. At E18.5, the fetal skeletal muscles of the various genetically modified mice exhibit more pronounced morphological alterations. At this time point, the skeletal muscle of a WT fetus (A-C) is mature with regularly developed muscle fascicles consisting of normal sized muscle fibers as well as inconspicuous bone having reached a normal state of mineralization. In a $RYR1^{+/-}$ fetus (D-F), skeletal muscle and bone are normally developed, thus, being similar to WT mice. In contrast, the skeletal muscle of a $RYR1^{-/-}$ (G,H) and a $Ca_v1.1^{-/-}$ (M,N) fetus, respectively, consists predominantly of small, unorganized myotubes with lack of a fascicular organization. In addition, bone of the hind limb of a $Ca_v1.1^{-/-}$ (M-O) fetus is impaired in development as evidenced by persisting hyaline cartilage while mineralization has not been initiated (arrows in M). At day E18.5 apoptosis is completely absent from all mutant strains as evidenced by the absence of nuclear immunoreaction in immunohistochemistry with anti-activated caspase-3. H&E staining (A, B, D, E, G, H, J, K, M, and N); original

magnification x100 (A, D, G, J, M) and x200 (B, E, H, K, N). Immunohistochemistry with rabbit anti-mouse activated caspase-3 (clone C92-605; BD Biosciences) and slight counterstaining with hemalum; original magnification x400. Scale bars correspond to 100 μm in all microphotographs.

https://doi.org/10.1371/journal.pone.0194428.g003

of heterozygous $RYR1^{+/-}$ animals (Fig 2D and 2E) was similar to WT fetuses, the hind limb muscles of homozygous $RYR1^{-/-}$ mutants (Fig 2G and 2H) were predominated by myotubes with only single muscle fibers of a decreased fiber caliber. In addition, there was no evidence for any organization of muscle fascicles in $RYR1^{-/-}$. At E14.5, morphological alterations in muscles obtained from$Ca_v1.1^{-/-}$ animals (Fig 2M and 2N) were similar to that of $RYR1^{-/-}$ mutants. However, in contrast to heterozygous $RYR1^{+/-}$ animals which were morphologically similar to the WT fetuses, the disorganization of muscle fascicles obtained from heterozygous $Ca_v1.1^{+/-}$ animals (Fig 2J and 2K) was similar to those of homozygous $Ca_v1.1^{-/-}$ mice (Fig 2M and 2N). Thus, homozygous $Ca_v1.1^{-/-}$ state displayed the most severe phenotype, with skeletal muscles consisting almost exclusively of small caliber myotubes and myoblasts while mature muscle fibers were virtually absent (Fig 2M and 2N). Apoptosis of a small fraction of myotubes has only been identified in the skeletal muscles of E14.5 $Ca_v1.1^{-/-}$ fetuses as evidenced by nuclear anti-activated caspase-3 staining (Fig 2O, arrows) while it was absent in the other fetuses.

At E18.5, WT and $RYR1^{+/-}$ muscles were normally developed and consisted predominantly of well-differentiated muscle fibers organized in fascicles (Fig 3A–3F), thus, being in line with our own recent study [28]. At this time point, the skeletal muscle of $RYR1^{-/-}$ fetuses consisted predominantly of myotubes and small, disorganized fibers accompanied by a severely affected fascicle formation, hinting a developmental retardation (Fig 3G and 3H). In contrast, the skeletal muscles of both heterozygous $Ca_v1.1^{+/-}$ fetuses (Fig 3J and 3K) and homozygous E18.5 $Ca_v1.1^{-/-}$ fetuses (Fig 3M and 3N) still exhibited signs of immaturity as characterized by a predominance of myoblasts and myotubes and only a fraction of muscle fibers showing evidence of a beginning organization into fascicles in heterozygous $Ca_v1.1^{+/-}$ fetuses (Fig 3J and 3K). In contrast, the skeletal muscle of homozygous E18.5 $Ca_v1.1^{-/-}$ fetuses (Fig 3M and 3N) completely persisted in immature state. In addition, maturation of bone of the hind limbs of homozygous E18.5 $Ca_v1.1^{-/-}$ fetuses (Fig 3; arrows in M) was markedly retarded with persistence of hyaline cartilage at a time point when mineralization of bones should be active.

Only discrete changes were observed in the expression of myogenic regulatory factors (MRFs) in $RYR1^{-/-}$ and $Ca_v1.1^{-/-}$ skeletal muscle at E14.5 and E18.5

The genes *Six1*, *Six4*, *Pax3*, *Pax7*, *Myf5*, *Myod1*, *Myog* and *Mrf4* encode canonical MRFs that affect the expression of multiple genes throughout skeletal muscle development [10]. We previously reported changes in the expression levels of several MRFs at E18.5 in $RYR1^{-/-}$ skeletal muscle [28]. In the present study, we investigated MRFs expression in limb skeletal muscle at E14.5 and E18.5. This was done via qRT-PCRs of samples from 6 $RYR1^{-/-}$, 6 $Ca_v1.1^{-/-}$ and 6 WT animals (Fig 4). At E14.5, a slight but significant downregulation of *Six1* (0.7-fold of WT) was observed in $RYR1^{-/-}$ samples and a stronger downregulation of *Mrf4* (0.33-fold of WT)–in the $Ca_v1.1^{-/-}$ samples with no significant changes in the other MRFs in both lines. However, in the $RYR1^{-/-}$ samples *Pax3* exhibited a tendency towards downregulation, which was significant at E18.5. No further statistically significant changes in the expression of any of the MRFs were found for the $RYR1^{-/-}$ and $Ca_v1.1^{-/-}$ samples at E18.5.

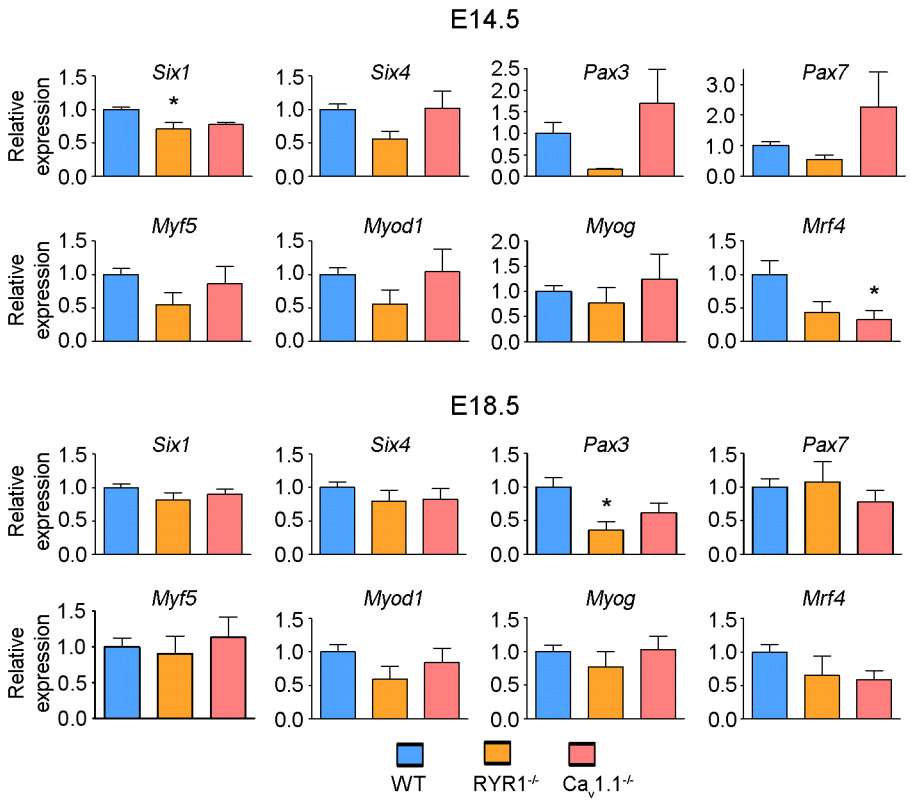

Fig 4. Comparison of the expression of MRFs in skeletal muscle from WT, $RYR1^{-/-}$ and $Ca_v1.1^{-/-}$ mice at E14.5 and at E18.5. Relative expression levels of *Six1*, *Six4*, *Pax3*, *Pax7*, *Myf5*, *Myod1*, *Myog* and *Mrf4* in WT, $RYR1^{-/-}$ and $Ca_v1.1^{-/-}$ samples (each n = 6) at E14.5 (upper part) and E18.5 (lower part) were obtained by qRT-PCR analyses, using *Cytb* as endogenous control. Expression levels of WT samples were set to 1. One way ANOVA with Bonferroni's Multiple Comparison tests were performed for each gene, *represents a p-value $\leq$ 0.05. Error bars are S.E.M.

https://doi.org/10.1371/journal.pone.0194428.g004

Attenuated $Ca_v1.1$ isoform-switch in $RYR1^{-/-}$ limb skeletal muscle at E14.5

It has been previously reported that a splice variant of $Ca_v1.1$ lacking exon 29 ($Ca_v1.1$ Δ29) is highly expressed in skeletal muscle during embryonic development and that its expression levels diminish at birth and almost disappear until the third week of postnatal development [33,34]. Unlike the full-length $Ca_v1.1$, which predominates in fully differentiated fibers and which only weakly conducts Ca^{2+} currents, the Δ29 variant is characterized by a much higher Ca^{2+} conductance and has been implicated in patterning of the neuromuscular junction during development [34]. To investigate whether the absence of RYR1 has an impact on the normal developmental pattern of $Ca_v1.1$ splice variants, we analyzed the relative expressions levels of the two $Ca_v1.1$ splice forms (full length and Δ29) in WT and $RYR1^{-/-}$ limb skeletal muscle. The region between exons 28 and 32 of the $Ca_v1.1$ transcript was amplified via PCR (Fig 5A), using cDNA from the limb skeletal muscles of 6 WT and 6 $RYR1^{-/-}$ animals at E14.5 and E18.5. The full length $Ca_v1.1$ transcript yielded a 343 bp PCR product and the Δ29 $Ca_v1.1$ transcript—a 286 bp PCR product. The PCR products were subjected to agarose gel electrophoresis (Fig 5B, S1 Fig), the intensities of the bands were measured and used for calculation of the relative amount of each splice variant as a percentage of the total $Ca_v1.1$ transcript (Fig 5C). At E14.5 each of the splice variants constituted approximately 50% of the total $Ca_v1.1$ transcript in the WT samples, whereas in the $RYR1^{-/-}$ samples the Δ29 $Ca_v1.1$ variant amounted for 70% of the total $Ca_v1.1$ transcript. At E18.5 the transcript levels for the full length $Ca_v1.1$ were

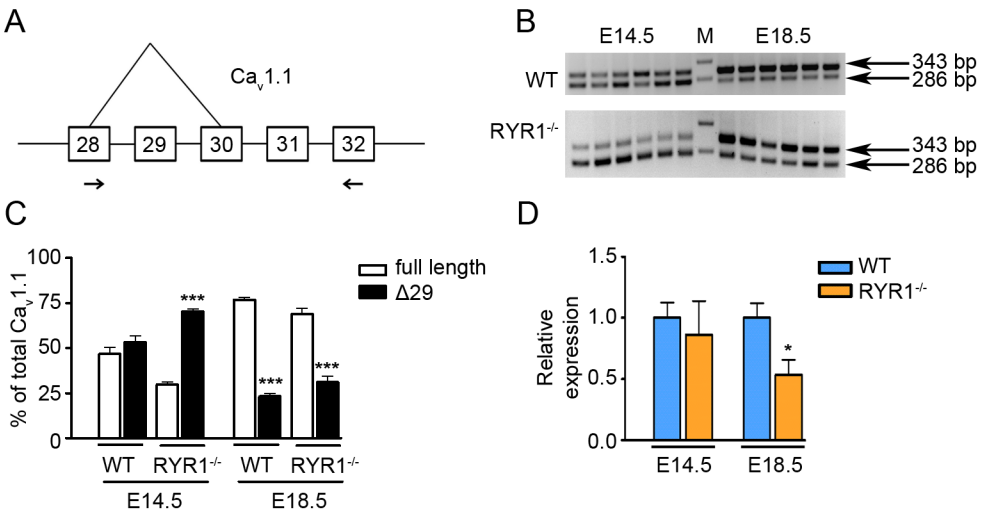

Fig 5. $Ca_v1.1$ splice variants in WT and $RYR1^{-/-}$ skeletal muscle. (A) Graphical representation of the genomic exon 29 vicinity of murine full-length and Δ29 $Ca_v1.1$ (NCBI Reference Sequence: NM_001081023.1) splice variants. Arrows indicate the primer binding positions used for amplification of exons 28–32. (B) PCR products of the full-length (343 bp) and Δ29 (286 bp) $Ca_v1.1$ splice variants. (C) Full-length (343 bp) and Δ29 (286 bp) splice variants as percentage of total $Ca_v1.1$ mRNA in limb skeletal muscle from WT and $RYR1^{-/-}$ animals at E14.5 and E18.5. (D) Relative expression of total $Ca_v1.1$ mRNA measured via qRT-PCR in $RYR1^{-/-}$ vs. WT skeletal muscle at E14.5 and E18.5, using *Cytb* as endogenous control. *t*-tests were performed for comparison of Δ29 vs. full-length splice variants (C) and for WT vs. $RYR1^{-/-}$ (D) in each group; * indicates *p* values <0.05 and *** *p* values < 0.001; error bars are S.E.M.

https://doi.org/10.1371/journal.pone.0194428.g005

significantly higher than those for Δ29 $Ca_v1.1$, in both WT and $RYR1^{-/-}$ (77% in WT and 69% in $RYR1^{-/-}$). However, qRT-PCR revealed an approximately 2-fold lower total level of $Ca_v1.1$ mRNA in $RYR1^{-/-}$ compared to WT limb skeletal muscle at E18.5. These results are in agreement with previous studies demonstrating a 2-fold reduced $Ca_v1.1$ protein expression, as well as a strong decrease of L-type Ca2+ current density and charge movements in skeletal muscle from $RYR1^{-/-}$ neonates [29,35,36]. The prolonged prevalence of $Ca_v1.1$ Δ29, as well as a reduced $Ca_v1.1$ expression in the absence of RYR1 is indicative of an impaired skeletal muscle development. These results also infer possible defects in proper neuromuscular junction formation that might have various downstream effects on the myogenic program.

Global transcriptome analyses reveal distinct profiles of $RYR1^{-/-}$ and $Ca_v1.1^{-/-}$ limb skeletal muscle at E18.5

In order to elucidate the global changes in gene expression that accompany secondary myogenesis in mouse limb skeletal muscle from E14.5 to E18.5, we performed microarray analyses (MAs). In particular, at each time point (E14.5 and E18.5) the skeletal muscles from the front and hind limbs of 3 littermates of each of the genotypes $RYR1^{+/+}$ (WT), $RYR1^{+/-}$ and $RYR1^{-/-}$, as well as $Ca_v1.1^{+/+}$ (WT), $Ca_v1.1^{+/-}$ and $Ca_v1.1^{-/-}$ were collected and used for total RNA extraction (Fig 6). After evaluation of their quality (S2 Fig), the RNAs were subjected to MAs, with each MA covering 41,345 probes.

In order to analyze whether the different genotypes, developmental stages, and biological replicates from the same genotype and stage, segregate into distinct groups on the basis of their variance in expression, a principal component analysis (PCA) was performed for all genes identified in the MAs. As Fig 7A shows, the most prominent separation is that between developmental stages (PC 1 = 47.2% variance). Only secondary is the separation within the E18.5 group (squares in Fig 7A) between homozygous ($Ca_v1.1^{-/-}$ or $RYR1^{-/-}$) mutants and the

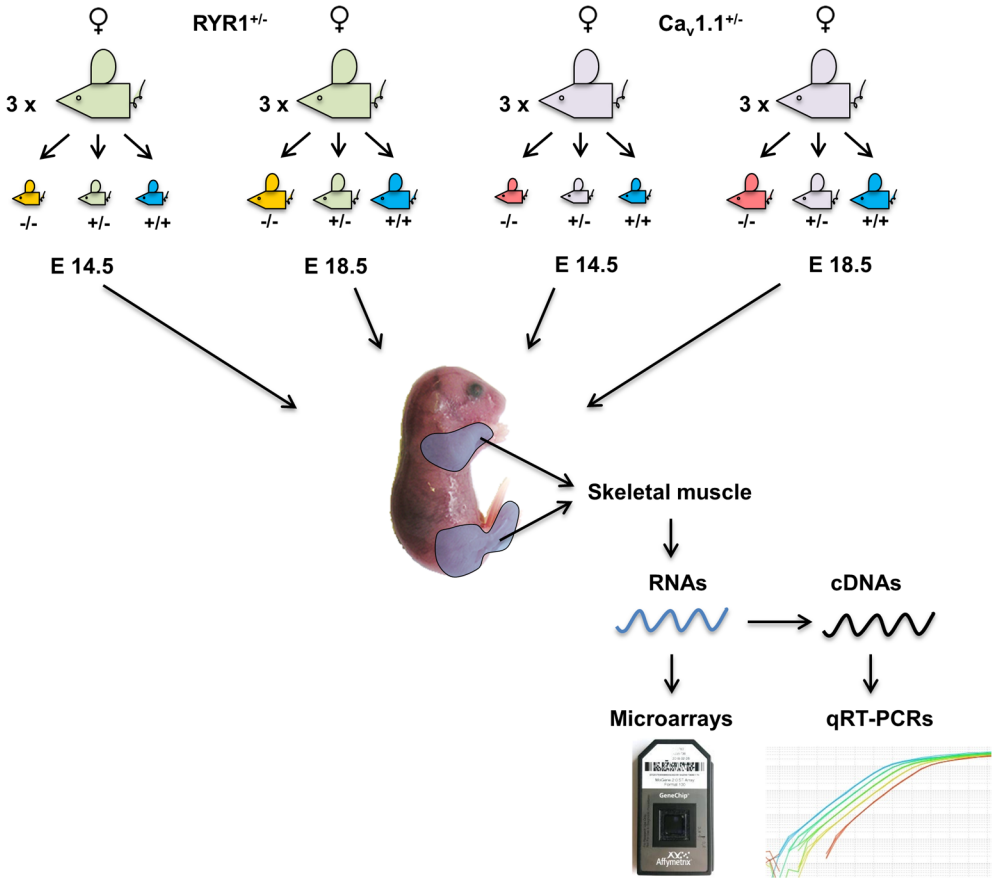

Fig 6. Schematic representation of the samples used in the present study and work flow for the subsequent gene expression analyses. Heterozygous $Ca_v1.1^{+/-}$ and $RYR1^{+/-}$ male and female animals were subjected to timed pairings. At E14.5 and E18.5 post coitum three pregnant females of each line were sacrificed and skeletal muscle samples were collected from the front and hind limbs of 3 littermates (n = 3) of each of the genotypes—WT, heterozygous ($Ca_v1.1^{+/-}$ or $RYR1^{+/-}$) and homozygous ($Ca_v1.1^{-/-}$ or $RYR1^{-/-}$) mutants. Samples were handled separately and used for total RNA extractions and subsequent MA and qRT-PCR analyses.

https://doi.org/10.1371/journal.pone.0194428.g006

other genotypes (PC 2 = 5.3% variance), which is most distinct for the $Ca_v1.1^{-/-}$ genotype (green squares in Fig 7A). In contrast, PCA revealed no clear separation of genotypes for the E14.5 stage. Thus, the PCA analysis demonstrates that the E18.5 limb skeletal muscle transcriptomes of the homozygous mutants share more similarity with each other than with any other analyzed genotype.

Our MAs focus on two aspects, first a developmental aspect, by performing comparisons of the same genotype for the two stages E14.5 and E18.5, as well as a genotype aspect, by performing comparisons within the same embryonic day but for distinct genotypes. In the first case we considered a gene as being differentially regulated between the two developmental groups when its p-value was ≤ 0.05 and when its linear FC was $\leq$-2 or $\geq$+2 (Fig 7B). In the other case (focus on genotype-specific changes) our criteria for classifying a gene as a DEG were an FC of $\leq$-1.5 or $\geq$+1.5, and a $p \leq 0.05$ (Fig 7C). Only DEGs meeting these criteria (Table 2, S1 Table) were subjected to further analysis. Furthermore, the samples from heterozygous ($RYR1^{+/-}$; $Ca_v1.1^{+/-}$) animals revealed only a handful of DEGs when compared to their WT littermates, at both E14.5 and E18.5. Therefore our further analysis focuses on the comparison of transcriptomic changes in homozygous mutant ($RYR1^{-/-}$; $Ca_v1.1^{-/-}$) vs. WT limb skeletal muscle.

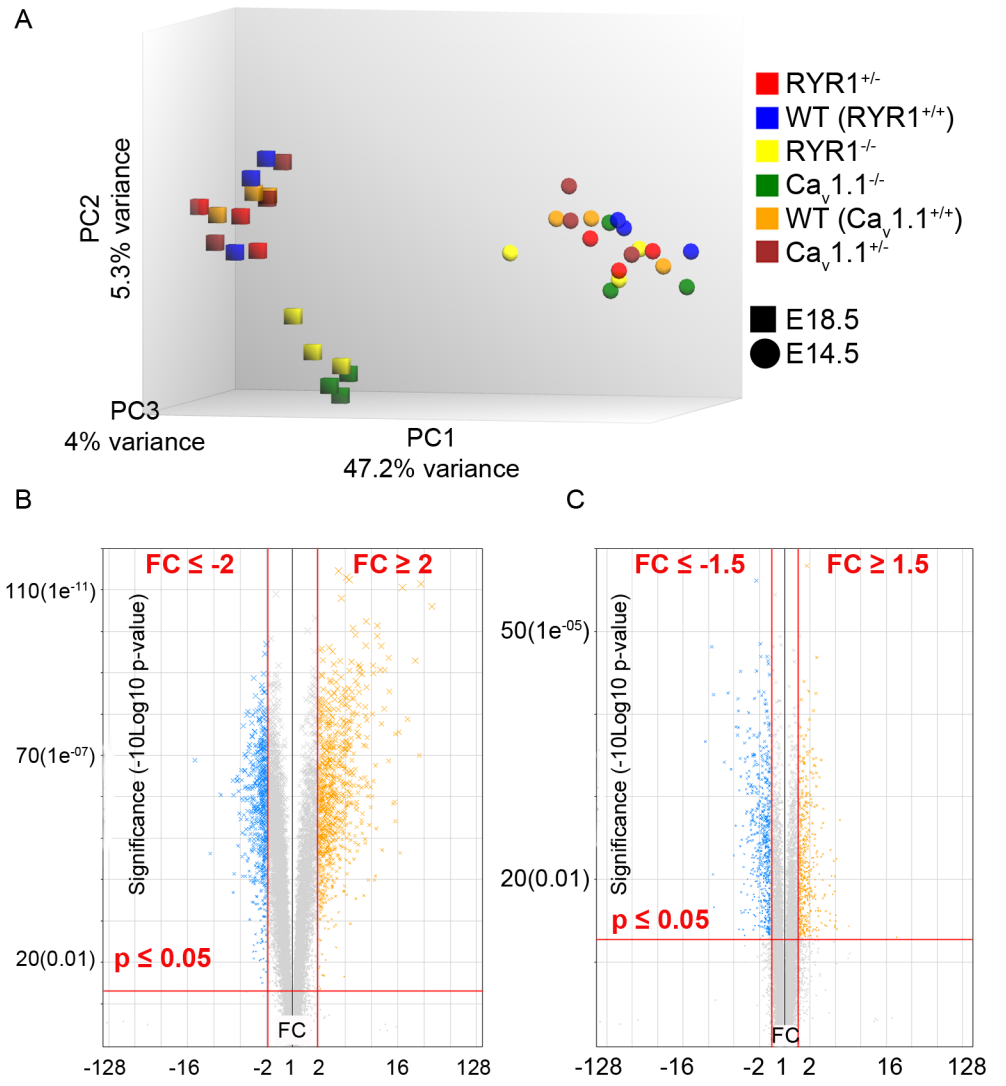

Fig 7. Initial MAs and DEGs analysis. (A) A principal component analysis (PCA) was performed for all samples with all their genes detected by the MAs via the Transcriptome Analysis Console 3.0 (Affymetrix®). (B) When comparing different developmental stages (E18.5 vs. E14.5), the cut-off criteria for being considered as DEG were an FC ≥ +2 or ≤-2, and a $p \leq 0.05$ (the example shown is from the comparison WT E18.5 vs. WT E14.5). (C) When comparing groups from the same developmental stage, the cut-off criteria were an FC ≥ +1.5 or ≤-1.5, and a $p \leq 0.05$ (the example shown is from the comparison $Ca_v1.1^{-/-}$ E18.5 vs. WT E18.5).

https://doi.org/10.1371/journal.pone.0194428.g007

Validation of the MAs via qRT-PCRs

Next, the results obtained using MA were validated via qRT-PCRs. For validation of the comparison of gene expression between E14.5 and E18.5, seven to eight down- or upregulated DEGs, covering a broad FC spectrum were randomly selected. Fig 8A–8C presents the results of this validation for WT, $RYR1^{-/-}$, and $Ca_v1.1^{-/-}$ samples, respectively. Due to the eminently lower number of DEGs detected by the MAs in E14.5 vs. E14.5 comparisons, fewer genes were used for the validation of $RYR1^{-/-}$ vs. WT and $Ca_v1.1^{-/-}$ vs. WT at this developmental stage (Fig 8D and 8E). Validation of the E18.5 vs. E18.5 comparisons comprised six ($RYR1^{-/-}$ vs. WT, Fig 8F) and seven ($Ca_v1.1^{-/-}$ vs. WT, Fig 8G) genes, respectively. As Fig 8 shows, the direction of changes in expression detected by our MAs, and for many of the genes also the FC magnitude,

Table 2. Differentially regulated genes for various comparisons of genotypes.

Test group	Comparisson(Test vs. Control group)	Total DEGs	Downregulated DEGs	Upregulated DEGs
WT	E18.5 vs. WT E14.5	1314	541	773
$RYR1^{+/-}$	E18.5 vs. $RYR1^{+/-}$ E14.5	1426	611	815
	E14.5 vs. WT E14.5	36	27	9
	E18.5 vs. WT E18.5	21	13	8
$RYR1^{-/-}$	E18.5 vs. $RYR1^{-/-}$ E14.5	812	311	501
	E14.5 vs. WT E14.5	61	32	29
	E18.5 vs. WT E18.5	493	304	189
$Ca_v1.1^{+/-}$	E18.5 vs. $Ca_v1.1^{+/-}$ E14.5	1079	433	646
	E14.5 vs. WT E14.5	8	5	3
	E18.5 vs. WT E18.5	33	10	23
$Ca_v1.1^{-/-}$	E18.5 vs. $Ca_v1.1^{-/-}$ E14.5	900	282	618
	E14.5 vs. WT E14.5	97	66	31
	E18.5 vs. WT E18.5	1047	571	476

https://doi.org/10.1371/journal.pone.0194428.t002

was firmly recapitulated by our quantitative PCR analysis. Therefore, we conclude that our results obtained using MAs give a reliable picture of the changes in expression in the various skeletal muscle samples.

Transcriptomes of $RYR1^{-/-}$ and $Ca_v1.1^{-/-}$ limb skeletal muscle deviate from WT already at E14.5

An important question in our analysis was about the time of onset of transcriptomic alterations during skeletal myogenesis when either RYR1 or $Ca_v1.1$ is absent. We therefore compared the E14.5 MA profiles of $RYR1^{-/-}$ and $Ca_v1.1^{-/-}$ limb skeletal muscle to those of their WT littermates. 61 DEGs were identified in the $RYR1^{-/-}$ samples and 97 DEGs in the $Ca_v1.1^{-/-}$ samples (Table 2, S1 Table). Interestingly, only two DEGs—the solute carrier family 44, member 5 (*Slc44a5*) and Der1-like domain family, member 3 (*Derl3*) were found in both $RYR1^{-/-}$ and $Ca_v1.1^{-/-}$ samples, suggesting that the absence of RYR1 or $Ca_v1.1$ at this early stage might affect distinct cellular processes. Indeed GO BP enrichment analysis revealed that processes related to innervation and to cellular transport were most significantly influenced in $RYR1^{-/-}$ samples (Fig 9A, S2 Table), whereas the most affected processes in $Ca_v1.1^{-/-}$ samples were associated with muscle contraction (Fig 9B, S2 Table). Heatmaps were generated for the DEGs related to the most significantly altered processes, i.e., "Regulation of neuron differentiation" in $RYR1^{-/-}$ samples (Fig 9C, S3 Table) and "Muscle contraction" in $Ca_v1.1^{-/-}$ samples (Fig 9D, S3 Table). Both heatmaps show a downregulation of all DEGs related to these two processes, with the only exception in $Ca_v1.1^{-/-}$ being *Myh6*, which encodes cardiac myosin heavy polypeptide 6, alpha.

Substantial overlap of $RYR1^{-/-}$ and $Ca_v1.1^{-/-}$ limb skeletal muscle transcriptomes at E18.5

To determine how the moderate changes found in the transcriptomes of $RYR1^{-/-}$ and $Ca_v1.1^{-/-}$ at E14.5 evolve until the later stage of secondary myogenesis, we performed analogous screens using samples from E18.5. Using WT E18.5 as the reference, 493 DEGs were identified in the $RYR1^{-/-}$ samples and 1,047 DEGs in the $Ca_v1.1^{-/-}$ samples (Table 2, S1 Table). 328 DEGs were shared by both $RYR1^{-/-}$ and $Ca_v1.1^{-/-}$ samples, which, with respect to the total number of DEGs identified in the E18.5 comparisons, is a significant overlap (66.5% of all $RYR1^{-/-}$ DEGs

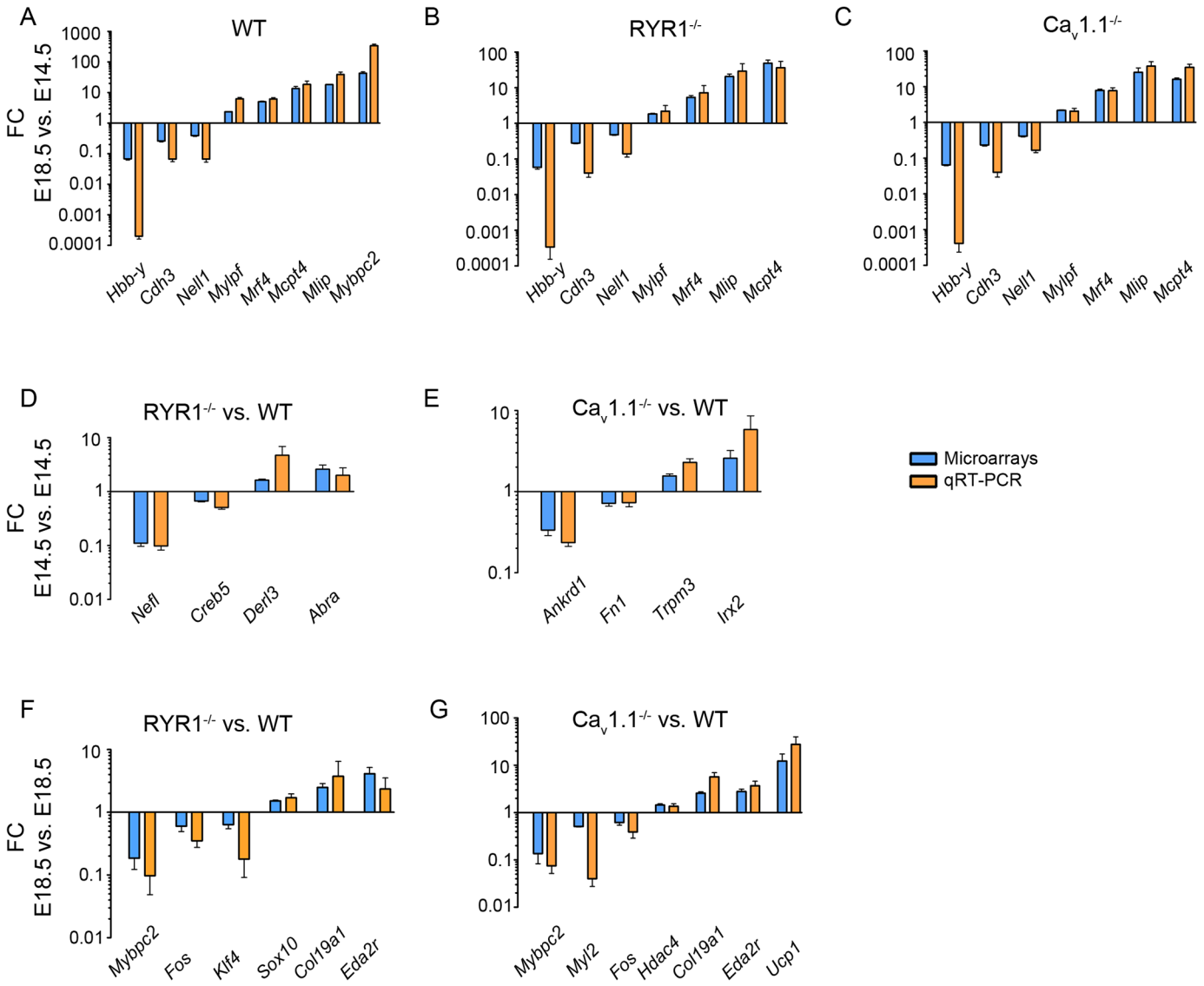

Fig 8. Validation of the MAs results via qRT-PCRs. (A-C) Validation of DEGs found in the comparison E18.5 vs. E14.5 for the same genotype. (A), WT vs. WT, 8 genes, n = 6 biological replicates per group; (B), $RYR1^{-/-}$ vs. $RYR1^{-/-}$, 7 genes, n = 3 biological replicates per group; (C), $Ca_v1.1^{-/-}$ vs. $Ca_v1.1^{-/-}$, 7 genes, n = 3 biological replicates per group. (D-E) Validation of selected genes found to be differentially regulated in E14.5 samples from $RYR1^{-/-}$ muscle (D) and $Ca_v1.1^{-/-}$ muscle (E), when compared to E14.5 WT. (D & E), 4 genes for each genotype comparison, n = 3 biological replicates per group. (F-G) Validation of selected genes found to be differentially regulated in E18.5 samples from $RYR1^{-/-}$ muscle (F) and $Ca_v1.1^{-/-}$ muscle (G), when compared to E18.5 WT. (F), 6 genes, n = 3 biological replicates per group; (G), 7 genes, n = 3 biological replicates per group. In all MA and qRT-PCR analyses the FCs of the control samples were set to 1. The relative expression levels obtained by qRT-PCR analysis were normalized to *Cytb*, which was used as endogenous control. Error bars are S.E.M.

https://doi.org/10.1371/journal.pone.0194428.g008

were identical to 31.3% of all $Ca_v1.1^{-/-}$ DEGs). These results reveal a substantial similarity in the transcriptomic profiles of $RYR1^{-/-}$ and $Ca_v1.1^{-/-}$ limb skeletal muscle at the final stages of embryogenesis and of secondary myogenesis. Among the DEGs shared by both mutants at E18.5 were members of signaling pathways with critical roles in skeletal muscle development, like the MAPK, PI3K-AKT, Wnt, cAMP and cGMP-PKG pathways (S4 Table). Further analysis of all DEGs shared by $RYR1^{-/-}$ and $Ca_v1.1^{-/-}$ at E18.5 using GO BP, demonstrated that the three most significantly affected processes were identical in both mutants and were all related to muscle contraction (Fig 10A and 10B, S5 Table). However, GO BP enrichment analysis also

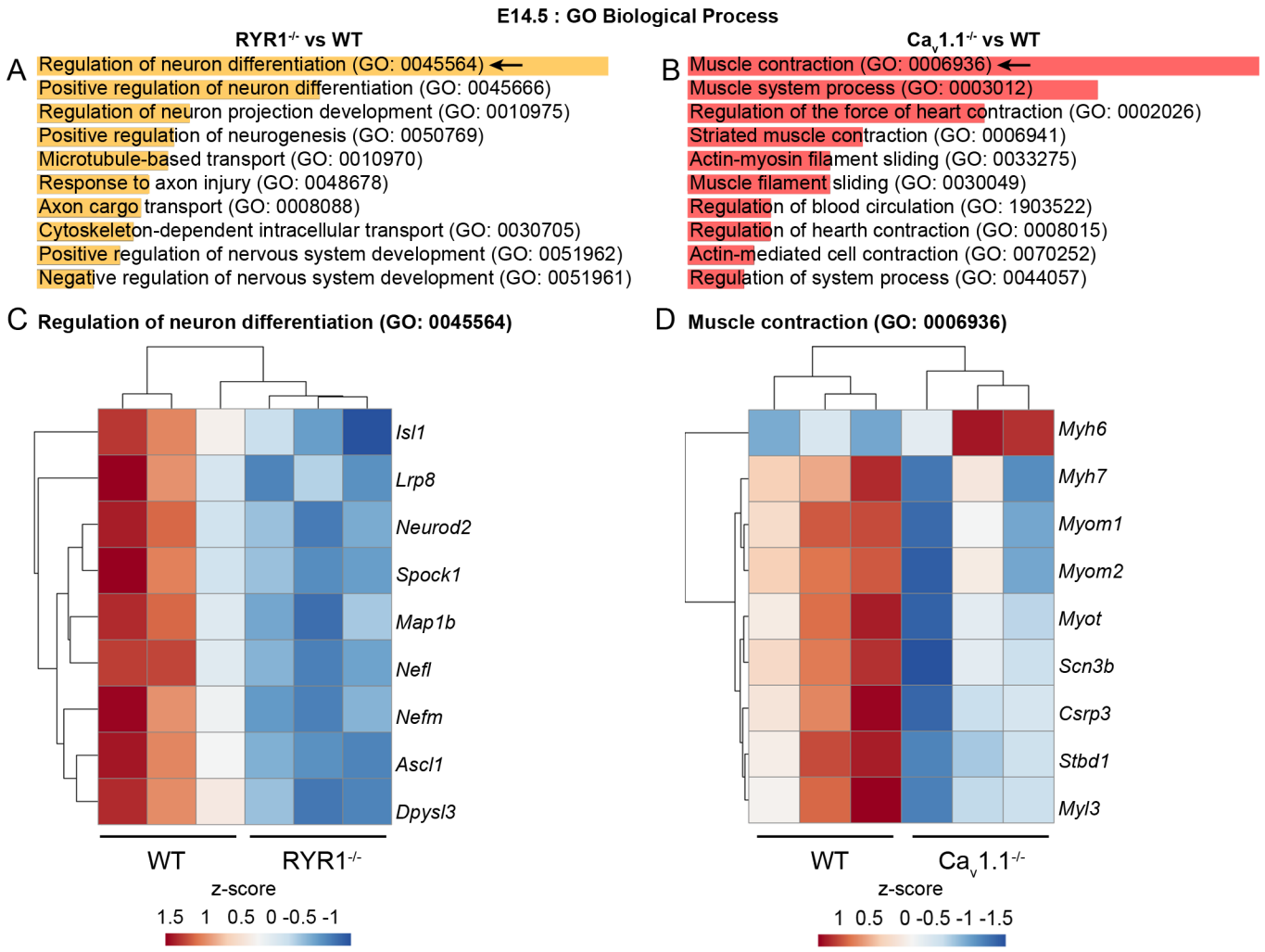

Fig 9. Biological processes affected by the $RYR1^{-/-}$ and $Ca_v1.1^{-/-}$ mutations at E14.5. GO BP enrichment analyses were performed for the DEGs identified in the $RYR1^{-/-}$ (A) and $Ca_v1.1^{-/-}$ (B) samples when compared to WT littermates samples at E14.5. The ten most significantly enriched categories for each analysis are shown. Arrows indicate categories presented as heat maps in (C) and (D). The enrichment analyses was performed via the Enrichr online tool [31], length of the bars represents the significance (p-value). Heatmaps were generated for the DEGs enriched in the "Regulation of neuron differentiation" biological process in $RYR1^{-/-}$ samples (C) and for the DEGs enriched in "Muscle contraction" biological process in $Ca_v1.1^{-/-}$ samples (D). The heatmaps were generated from the MAs intensity levels of each gene via ClustVis [32]. Hierarchical average linkage clustering using the Euclidean distance was performed for all rows and columns.

https://doi.org/10.1371/journal.pone.0194428.g009

generated assignments of DEGs to processes which were distinct in $RYR1^{-/-}$ and $Ca_v1.1^{-/-}$. For instance, highly enriched in the $RYR1^{-/-}$ samples were genes related to extracellular matrix and structure organization, while a group of DEGs in $Ca_v1.1^{-/-}$ samples is related to fatty acid and lipid metabolism. To appreciate the direction in which these processes were altered in the two mutants, heatmaps were constructed for the DEGs involved in *Muscle contraction* (as stated above the most significantly enriched biological process for both groups; Fig 10C, S6 Table). Heat maps were also generated for "Extracellular matrix organization", using the DEGs from $RYR1^{-/-}$ samples (Fig 10D, S7 Table) and for "Acylglycerol metabolic process", using the DEGs from $Ca_v1.1^{-/-}$ samples (Fig 9E, S8 Table). As the heat map in Fig 10C shows, a very large proportion of genes (44 of the 49 DEGs) assigned by GO BP to the process of "Muscle contraction" were downregulated in $RYR1^{-/-}$, in $Ca_v1.1^{-/-}$, or in both mutants. Only 5 DEGs were positively regulated (Fig 10C). A significant fraction of the negatively regulated DEGs encode

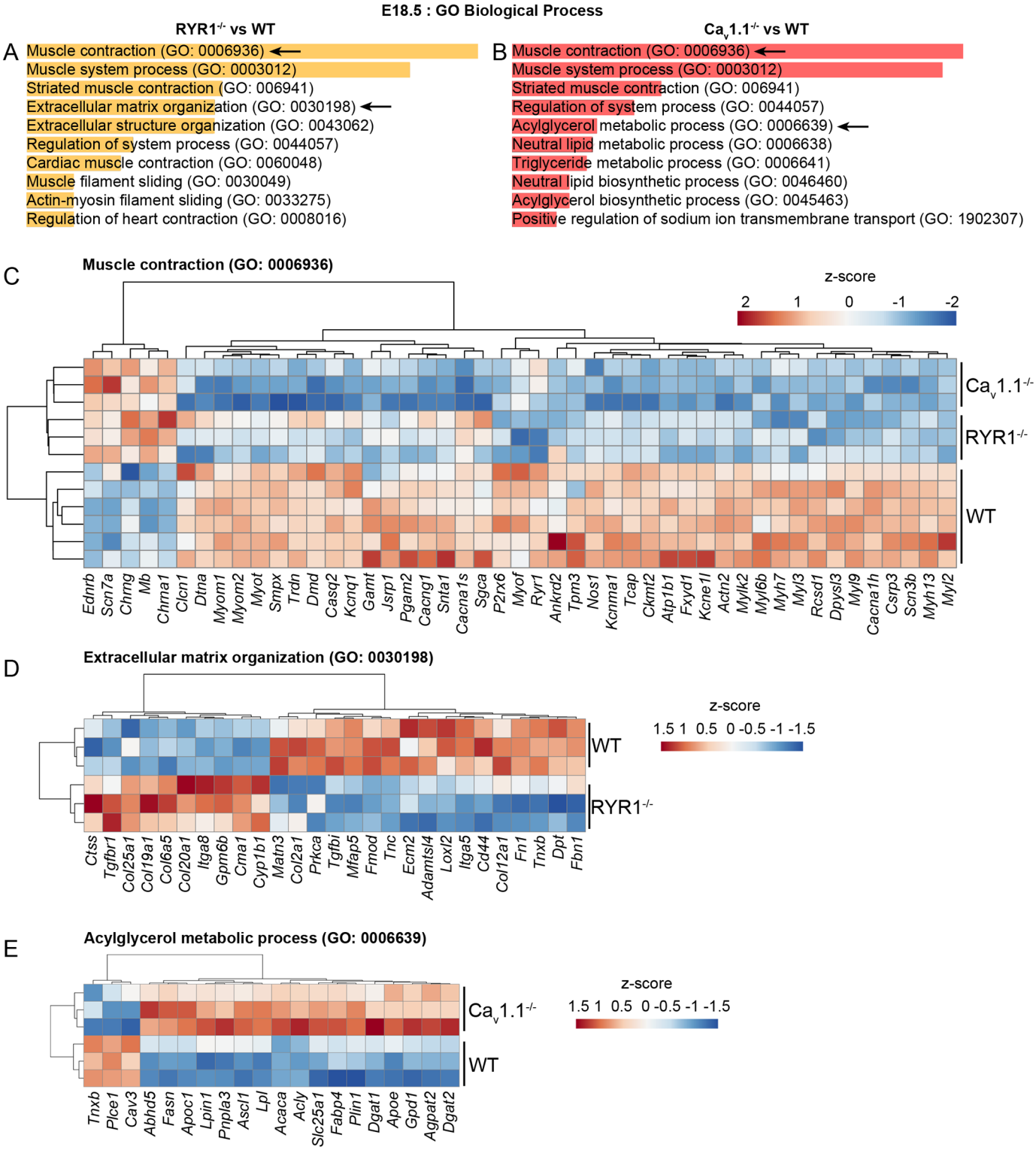

Fig 10. Biological processes affected by the $RYR1^{-/-}$ and $Ca_v1.1^{-/-}$ mutations at E18.5. GO BP enrichment analyses were performed for the DEGs identified in the $RYR1^{-/-}$ (A) and $Ca_v1.1^{-/-}$ (B) samples with their E18.5 WT littermates serving as reference. The ten most significantly enriched categories for each analysis are shown. Arrows indicate categories presented as heat maps in (C), (D) and (E). The enrichment analyses was performed via the Enrichr online tool [31], the length of the bars corresponds to the significance (p-value). Heatmaps were generated for the DEGs enriched in the "Muscle contraction" biological process in $RYR1^{-/-}$ and $Ca_v1.1^{-/-}$ samples (C); for the DEGs enriched in "Extracellular matrix organization" biological process in $RYR1^{-/-}$ samples (D); and for the DEGs enriched in "Acylglycerol metabolic process" biological process in $Ca_v1.1^{-/-}$ samples (E). Heatmaps were generated from the MAs intensity levels of each included gene via ClustVis [32]. Hierarchical average linkage clustering using the Euclidean distance was performed for all rows and columns.

https://doi.org/10.1371/journal.pone.0194428.g010

constituents of the sarcomere, like *Myl2*, *Myl3*, *Myl6b*, *Myl9*, *Myh3*, *Myh7*, *Csrp3*, *Tcap*, *Tpm3*, *Myom1* and *Myom2*, which explains the scarcity of myofibrils and probably also the abnormalities in sarcomere arrangement in limb skeletal muscle from $RYR1^{-/-}$ and $Ca_v1.1^{-/-}$ mice at the perinatal stage [24,27].

17 out of the 27 DEGs related to "Extracellular matrix organization" were negatively regulated in $RYR1^{-/-}$ compared to WT samples (Fig 10D). Among the 10 positively regulated genes four encoded collagens, hinting to potential changes in the composition of the ECM in $RYR1^{-/-}$ limb skeletal muscle.

The vast majority, 17 out of 20, of the DEGs relating in the enrichment analysis to the "Acylglycerol metabolic process", displayed a higher expression level in $Ca_v1.1^{-/-}$ muscle when compared to their WT littermates (Fig 10E). We therefore assume the presence of an enhanced lipid metabolism in limb skeletal muscle of E18.5 $Ca_v1.1^{-/-}$ mice.

The transcriptome of WT and mutant skeletal muscle at E18.5 vs. E14.5

In order to compare the skeletal muscle transcriptome of the E18.5 stage to that at E14.5, all DEGs identified in the E18.5 vs. E14.5, same-genotype comparison (WT vs. WT; $RYR1^{-/-}$ vs. $RYR1^{-/-}$; $Ca_v1.1^{-/-}$ vs. $Ca_v1.1^{-/-}$) were subjected to GO BP and WP enrichment analysis (Fig 11, S9 Table). In all three genotypes GO BP identified "Muscle contraction (GO:0006936)" as the

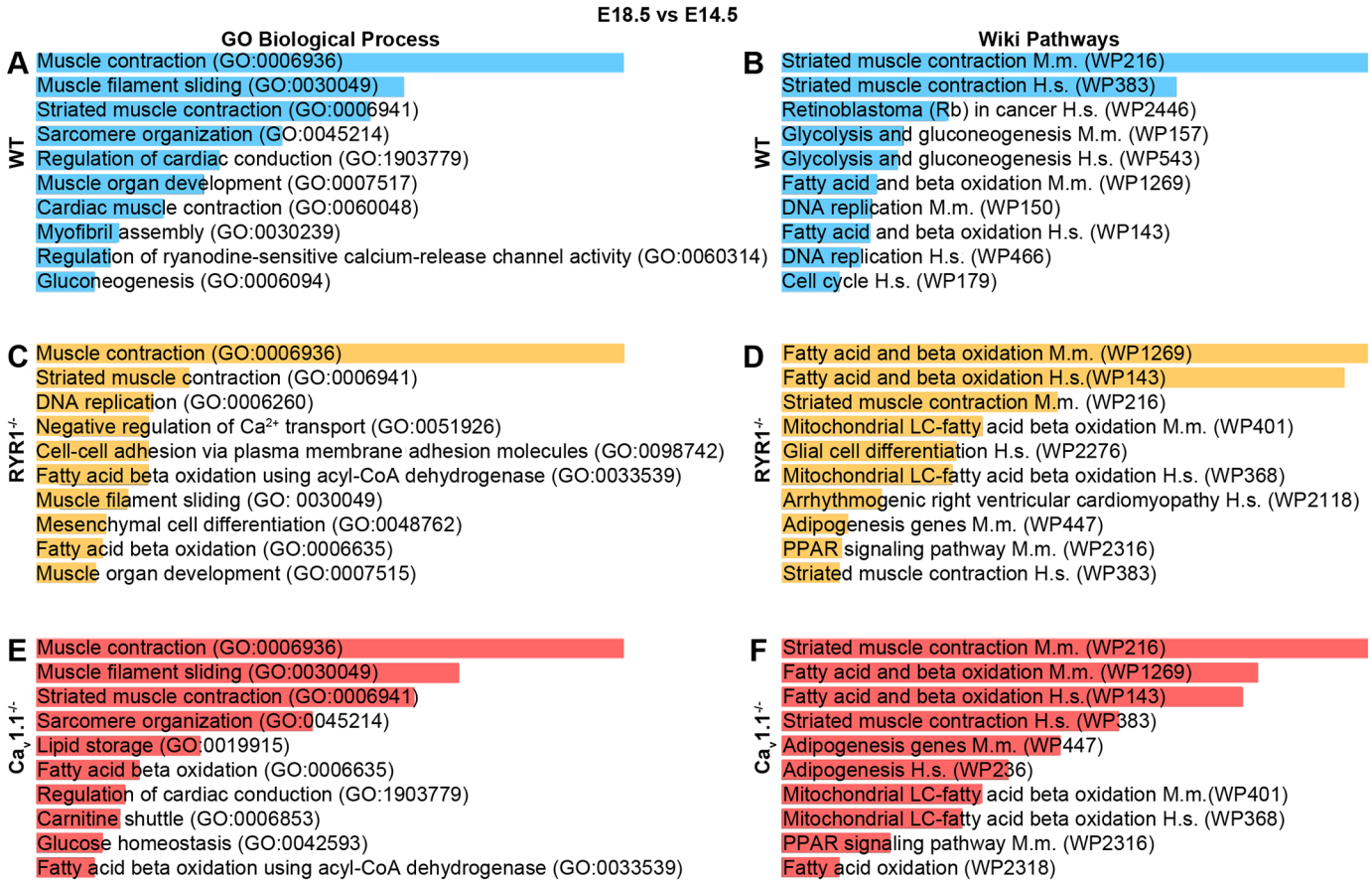

Fig 11. Analysis of all DEGs found in skeletal muscle development from E14.5 to E18.5. GO BP (A, C and E) and Wiki Pathways (B, D, F) enrichment analyses of all DEGs found in WT (A, B), $RYR1^{-/-}$ (C, D) and $Ca_v1.1^{-/-}$ (E,F) from E14.5 (control) to E18.5. The ten most significantly enriched categories for each analysis are shown. Enrichment analyses (A–F) were performed via the Enrichr online tool [31], length of the bars is proportional to the significance (p-value).

https://doi.org/10.1371/journal.pone.0194428.g011

most significantly involved biological process. In the case of E18.5 WT vs. E14.5 WT the GO BP enrichment analysis implicated additional processes related to muscle organization and contraction, which were only marginally represented in the analyses for $RYR1^{-/-}$ or $Ca_v1.1^{-/-}$ muscle. On the other hand, both $RYR1^{-/-}$ and $Ca_v1.1^{-/-}$ samples showed enrichment of DEGs involved in processes related to fatty acid metabolism and β-oxidation. Furthermore, $RYR1^{-/-}$ samples also exhibited an enrichment of DEGs involved in "DNA replication (GO:0006260)", "Negative regulation of calcium ion transport (GO:0051926)", "Cell-cell adhesion via plasma-membrane adhesion molecules (GO:0098742)", and "Mesenchymal cell differentiation (GO:0048762)". $Ca_v1.1^{-/-}$ samples, on the other hand, showed a specific enrichment in "Lipid storage (GO:0019915)", "Carnitine shuttle (GO:0006853)" and "Glucose homeostasis (GO:0042593)". The WP enrichment analyses revealed "Striated muscle contraction Mus musculus (WP216)" as the most-significantly engaged process in WT and $Ca_v1.1^{-/-}$ samples, whereas in the $RYR1^{-/-}$ samples "Fatty acid and beta oxidation Mus musculus (WP1269)/ Homo sapiens (WP143)" were more significantly implicated. Additional pathways which were significantly enriched in WT samples were related to glucose metabolism, DNA replication and cell cycle, whereas the $RYR1^{-/-}$ or $Ca_v1.1^{-/-}$ samples exhibited a more prominent enrichment in processes related to fat and energy metabolism.

The E18.5 vs. E14.5 comparison reveals overlap but also genotype-specific DEGs between WT, $RYR1^{-/-}$ and $Ca_v1.1^{-/-}$ limb skeletal muscle

One of our major objectives was to compare the global expression changes occurring from E14.5 to E18.5 in WT, $RYR1^{-/-}$ and $Ca_v1.1^{-/-}$ skeletal muscle. Therefore, we inspected how many DEGs were shared and how many were specifically regulated in the development of WT, $RYR1^{-/-}$ and $Ca_v1.1^{-/-}$ limb skeletal muscle (Fig 12A). This analysis revealed 429 common DEGs with changed expression levels from E14.5 to E18.5 in all examined genotypes, 169 DEGs shared between WT and $RYR1^{-/-}$ samples, 164 DEGs shared between WT and $Ca_v1.1^{-/-}$ samples and 100 DEGs shared between $RYR1^{-/-}$ and $Ca_v1.1^{-/-}$ samples. Moreover, 483 DEGs were specifically found only in the WT development, 91 DEGs—only in the $RYR1^{-/-}$ and 171 DEGs—only in the $Ca_v1.1^{-/-}$ development.

To better understand which pathways, processes and structures were influenced by the DEGs of a particular genotype they were subjected to WP, GO BG and GO CC enrichment analyses (Fig 12B–12J, S10 Table). For the WT-specific DEGs the WP enrichment analysis highlighted "miRs in muscle cell differentiation Homo sapiens (WP2012)" as well as other miRNA-related pathways and pathways related to cell cycle and signal transduction. Analyzing the $RYR1^{-/-}$-specific DEGs, the WP enrichment analysis identified endochondral ossification, BMP signaling and focal adhesion as significantly affected pathways, whereas in $Ca_v1.1^{-/-}$ these were pathways related to adipogenesis and lipid metabolism.

Similar results were obtained by the GO BP analysis, identifying "Positive regulation of rRNA processing (GO:2000234)" and several muscle- and cell cycle-related processes as highly enriched with WT-specific DEGs. "Chondrocyte differentiation (GO:0002062)", among other developmental processes, was enriched with $RYR1^{-/-}$-specific DEGs while "Acylglycerol acyl chain remodeling (GO:0036155)" and other lipid and fatty acid metabolic processes were enriched with $Ca_v1.1^{-/-}$-specific DEGs. The GO CC enrichment analysis indicated specific changes in the "Sarcolemma (GO:0042383)" and other muscle-specific structures like "Costamere (GO:0043034)", "Sarcomere (GO:0030017)", "I band (GO:0031674)", and "Z disc (GO:0030017)" in the WT-specific DEGs analysis. In the GO CC enrichment analysis of the $RYR1^{-/-}$-specific DEGs the structures "Postsynaptic membrane (GO:0045211)", "Acetylcholine gated channel complex (GO:0005892)" and "Voltage-

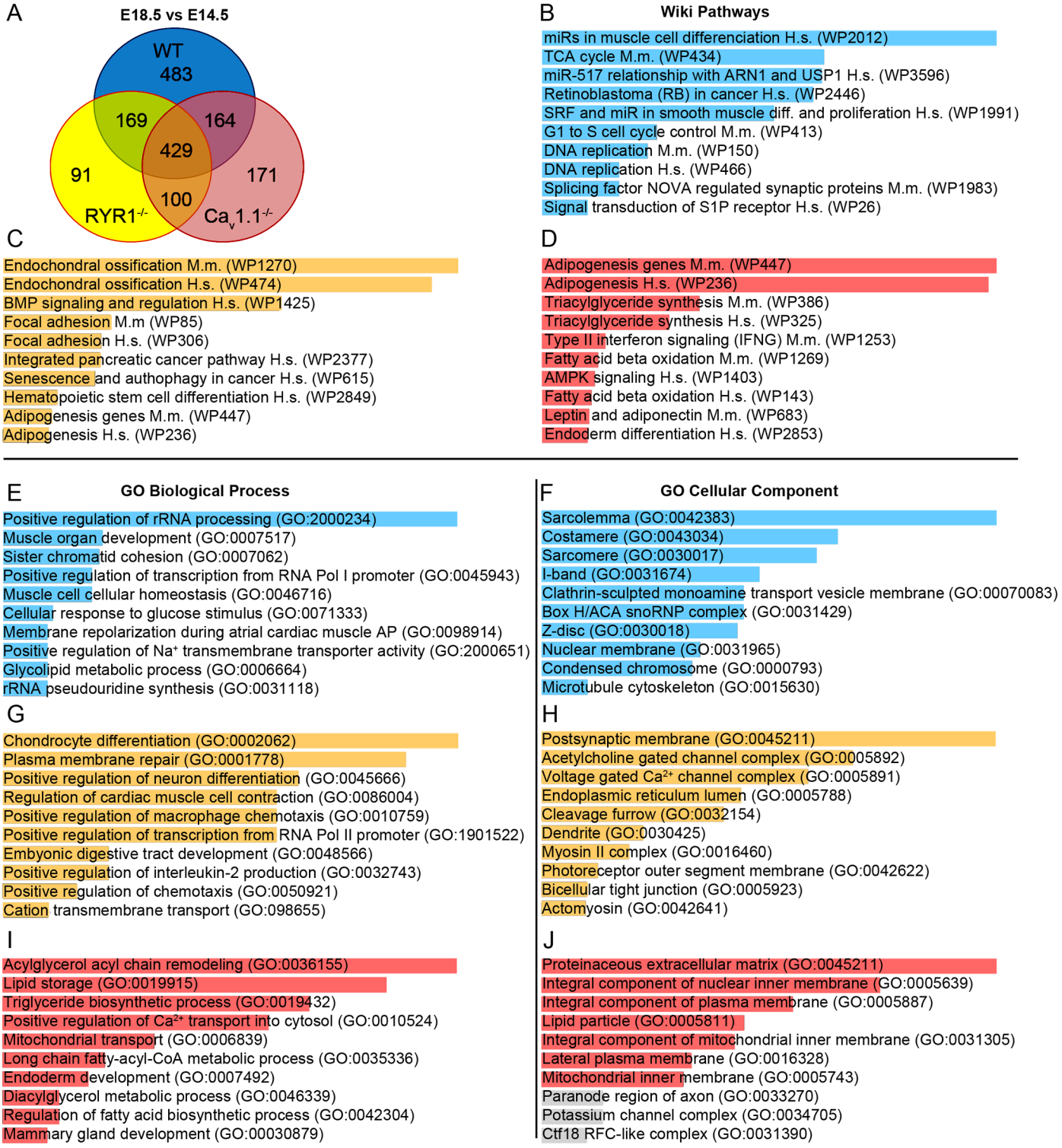

Fig 12. DEGs specific for the E14.5 to E18.5 development of WT, $RYR1^{-/-}$ or $Ca_v1.1^{-/-}$ skeletal muscle. (A) A Venn diagram, showing the number of DEGs identified in the MA analyses at E18.5 compared to E14.5 in WT, $RYR1^{-/-}$ and $Ca_v1.1^{-/-}$ limb skeletal muscle. Numbers in the overlapping and non-overlapping areas represent the amount of shared and not shared DEGs between genotypes, respectively. Wiki Pathways (B, C, D), GO BP (E, G, I) and GO CC (F, H, J) enrichment analyses of the DEGs found exclusively in WT (483 DEGs, blue charts), $RYR1^{-/-}$ (91 DEGs, yellow charts) and $Ca_v1.1^{-/-}$ (171 DEGs, red charts) from E14.5 (control) to E18.5, respectively. The ten most significantly enriched categories for each analysis are shown. Enrichment analyses (B–J) were performed via the Enrichr online tool [31], length of the bars is proportional to the significance (p-value). Gray bars in (J) indicate a p-value ≥ 0.05.

https://doi.org/10.1371/journal.pone.0194428.g012

gated Ca^{2+} channel complex (GO:0005891)" had the highest significance; and the "Proteinaceous extracellular matrix (GO:0045211)", "Integral component of nuclear inner membrane (GO:0005639)" and "Integral component of plasma membrane (GO:0005887)" were the top three cellular structures, enriched with $Ca_v1.1^{-/-}$-specific DEGs.

These results show, not unexpected [28], that the mutants recapitulate only a part of the transcriptomic changes associated with the development from E14.5 to E18.5 in WT skeletal muscle. However, the distinct transcriptomes of $RYR1^{-/-}$ and $Ca_v1.1^{-/-}$ muscles and the resulting differences in the allocation of DEGs to cellular processes also imply, from a causative point of view, that there is more to it than the mere absence of contraction and of the associated mechanical movement. Our data thus suggest functions additional to excitation-contraction coupling, of the two Ca^{2+} channels during skeletal muscle development. Recent experiments reported by other groups suggest distinct, extra-contractile functions of RYR1 and $Ca_v1.1$ in skeletal muscle development (detailed in Discussion).

Differential expression of microRNAs (miRNA) during limb secondary myogenesis

Two of the pathways significantly enriched with DEGs in the WP analysis (Fig 12B), displayed changes in miRNA expression in E18.5 vs. E14.5 for WT but not for $RYR1^{-/-}$ or $Ca_v1.1^{-/-}$ limb skeletal muscle, suggesting that miRNAs are part of the regulatory repertoire on which the two Ca^{2+} channels impart during secondary myogenesis. A further analysis of the DEGs participating in the "miRs in muscle cell differentiation Homo sapiens (WP2012)" pathway revealed 10 genes to be differentially expressed in WT samples and only 3 in $RYR1^{-/-}$ or $Ca_v1.1^{-/-}$ samples from E14.5 to E 18.5 (Fig 13A). Among the DEGs found only in WT are genes encoding modulators of some of the canonical MRFs like *Myod*, *Myf5* and *Pax7*; as well as 2 muscle-specific miRNAs (Myomirs), Mir206 and Mir133a-2, both known to be involved in muscle differentiation [37,38]. These results prompted us to analyze the MA expression levels of all differentially regulated miRNAs detected in E18.5 vs. E14.5 comparisons in WT, $RYR1^{-/-}$ and $Ca_v1.1^{-/-}$ samples (Fig 13B, Table 3). 61 miRNAs were differentially expressed in WT skeletal muscle, of which 16 were present also in the in $Ca_v1.1^{-/-}$ and 3 in the $RYR1^{-/-}$ samples. Additionally, we found one differentially expressed miRNA in $RYR1^{-/-}$ and 4 in $Ca_v1.1^{-/-}$, but not in WT muscle. A hierarchical clustering analysis displayed a clear grouping of the WT samples at E18.5 according to their miRNAs expression profiles (Fig 13B). A partial clustering was observed for the $RYR1^{-/-}$ and $Ca_v1.1^{-/-}$ samples at E18.5 on one side, and all samples at E14.5 on the other, wherein one $RYR1^{-/-}$ E18.5 sample was clustered closer to the E14.5 samples than to the other E18.5 samples. Notably, 56 miRNAs were upregulated and only 5 miRNAs were downregulated in the WT samples at E18.5 compared to E14.5. A similar tendency, but to a smaller extent, was observed for most $RYR1^{-/-}$ and $Ca_v1.1^{-/-}$ samples, however for most miRNAs no significant changes in expression were detected. Apart from the Myomirs, the MAs identified at least another 22 miRNAs, implicated in muscle development and in various myopathies, to be differentially expressed in WT samples during secondary myogenesis (Table 3). Interestingly, 32 (i.e., 52% of all) of the identified miRNAs which were upregulated in E18.5 relative to E14.5, in WT have been found by others to be downregulated in ageing skeletal muscle [39], suggesting that these miRNAs might have important roles during skeletal muscle development and during subsequent adaptation or alteration. Moreover, 26 (43% of all) of the identified miRNAs originate from a miRNA cluster, located within the imprinted *Dlk-Dio3* genomic region on chromosome 12. This region might be of eminent importance for skeletal muscle development.

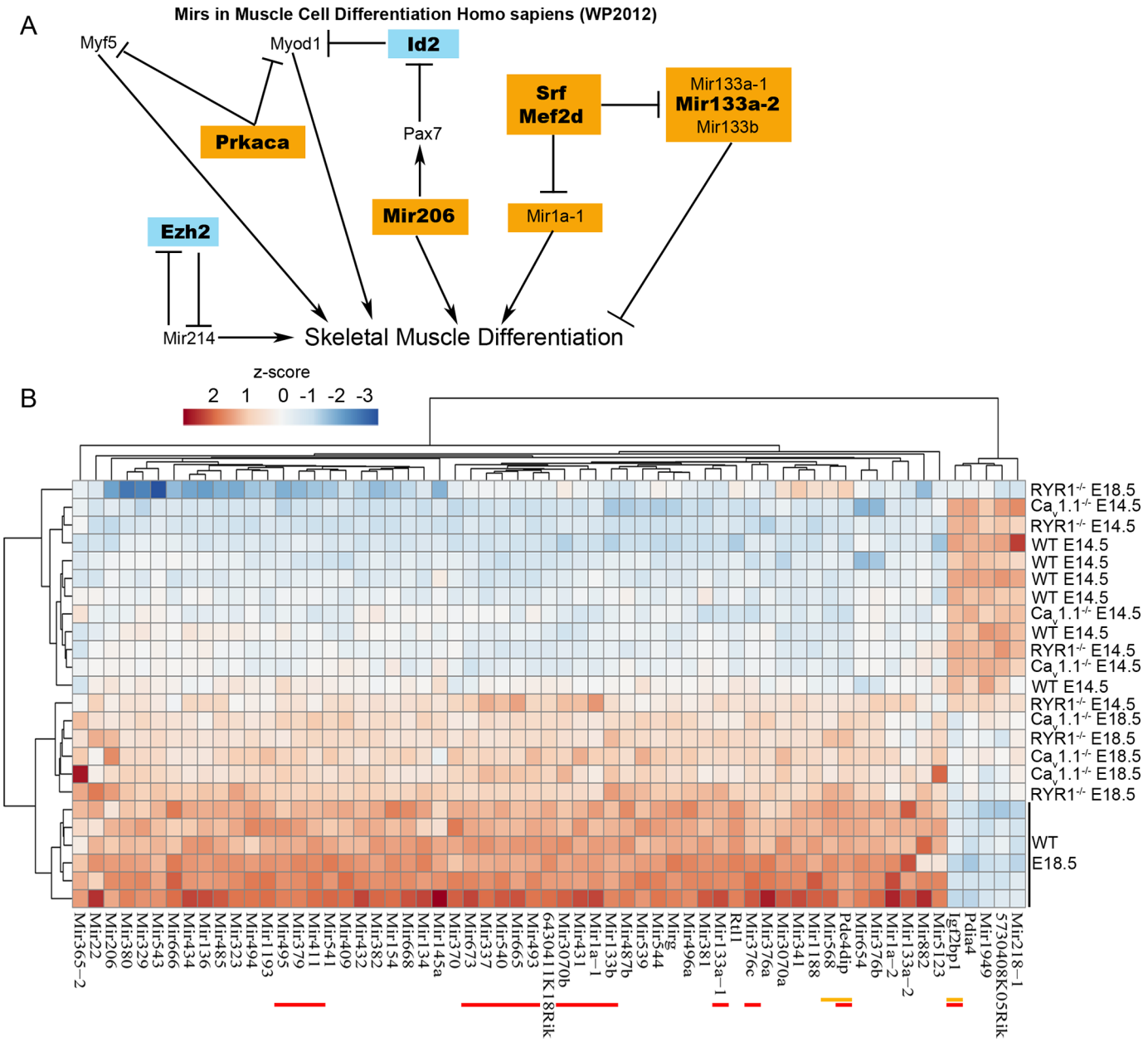

Fig 13. miRNAs identified by the MAs during WT skeletal muscle development. (A) Up (orange) and down (blue) regulated DEGs identified by the MAs for E18.5 vs. E14.5 (E14.5 is control) taking part in the Wiki pathway "Mirs in Muscle Cell Differentiation Homo sapiens (2012)". DEGs regulated only in WT samples from E14.5 to E18.5 are shown in bold. (B) A heat map of all miRNAs, found to be differentially regulated at E18.5 compared to E14.5 in WT samples. Each row represents one biological replicate. miRNAs, found to be differentially regulated from E14.5 to E18.5 also in $RYR1^{-/-}$ samples, are underlined in yellow, in the $Ca_v1.1^{-/-}$ samples in red, and in both $RYR1^{-/-}$ and $Ca_v1.1^{-/-}$ samples in yellow and red, respectively. The heatmap was generated from the MAs intensity levels of each of the Mir genes via ClustVis [32].

https://doi.org/10.1371/journal.pone.0194428.g013

Discussion

In this study we analyzed the histological and transcriptomic changes occurring in the developing limb skeletal muscle in the absence of RYR1 or $Ca_v1.1$. We have previously shown that, besides the known fact that homozygous loss of RYR1 ($RYR1^{-/-}$) is associated with severely altered skeletal muscle structure at E18.5, gene expression at this later stage displays a

Table 3. miRNAs differentially regulated from E14.5 to E18.5 in WT, $RYR1^{-/-}$ and $Ca_v1.1^{-/-}$.

Description	Gene Symbol	FC E18.5 vs. E14.5			Muscle-related functions	Reference
		WT	$RYR1^{-/-}$	$Ca_v1.1^{-/-}$		
Downregulated miRNAs						
microRNA 1949	Mir1949	-3.25	-	-		
insulin-like growth factor 2 mRNA binding protein 1; microRNA 3063	Igf2bp1	-3.23	-3	-2.43		
protein disulfide isomerase associated 4; microRNA 704	Pdia4	-2.59	-	-		
microRNA 218–1	Mir218-1	-2.58	-	-	involved in muscle-bone communication and Wnt signaling	[40]
RIKEN cDNA 5730408K05 gene; microRNA 5136	5730408K05Rik	-2.1	-	-		
Upregulated miRNAs						
MyoMirs						
microRNA 206	Mir206	2.08	-	-	promotes myoblast entry into terminal differentiation	[37]
microRNA 133b	Mir133b	2.73	-	2.12	enhances myoblast proliferation	[38]
microRNA 133a-2	Mir133a-2	3.69	-	-	enhances myoblast proliferation	[38]
microRNA 1a-2	Mir1a-2	4.01	-	-	positive roles in muscle development	[37]
microRNA 133a-1	Mir133a-1	5.36	-	2.83	enhances myoblast proliferation	[38]
microRNA 1a-1	Mir1a-1	6.29	-	2.32	positive roles in muscle development	[37]
miRNAs encoded in the Dlk-Dio3 genomic region						
microRNA 323	**Mir323**	**2.22**	-	-		
microRNA 668	**Mir668**	**2.32**	-	-		
microRNA 134; miRNA containing gene	**Mir134**	**2.35**	-	-	**possibly targets *Pax7* and *Myf5***	[41]
microRNA 485; miRNA containing gene	**Mir485**	**2.4**	-	-		
microRNA 494	**Mir494**	**2.42**	-	-		
microRNA 673	**Mir673**	**2.48**	-	**2.24**		
microRNA 544	**Mir544**	**2.5**	-	-		
microRNA 382	**Mir382**	**2.53**	-	-	**increased in Becker muscular dystrophy**	[42]
microRNA 666	**Mir666**	**2.55**	-	-		
microRNA 539	**Mir539**	**2.58**	-	-	**disregulated in DMD dogs**	[43]
microRNA 541	**Mir541**	**2.71**	-	-		
microRNA 381	**Mir381**	**2.9**	-	-	**implicated in muscle differentiation**	[44]
microRNA 487b	**Mir487b**	**2.98**	-	-	**delays myogenic differentiation in C2C12**	[45]
microRNA 431	**Mir431**	**2.98**	-	**2**	**promotes differentiation and regeneration of old skeletal muscle**	[46]
miRNA containing gene; microRNA 410; microRNA 412; microRNA 369	**Mirg**	**3**	-	-		
microRNA 409	**Mir409**	**3.17**	-	-	**upregulated in nemaline myopathy**	[47]
microRNA 495	**Mir495**	**3.5**		**2.4**		
microRNA 496a	**Mir496a**	**3.51**	-	-		
microRNA 379	**Mir379**	**3.8**	-	**2.28**		
microRNA 411	**Mir411**	**3.8**	-	**2.64**	**involved in myogenic proliferation in FSHD and rhabdomyosarcoma**	[48,49]
microRNA 341	Mir341	2.15	-	-		
microRNA 380	Mir380	2.57	-	-		
microRNA 654	Mir654	2.85	-	-		
microRNA 154	Mir154	3.2	-	-	downregulated by TNF-α in skeletal muscle differentiation	[50]
microRNA 376c	Mir376c	3.35	-	3.34		

(*Continued*)

Table 3. (Continued)

Description	Gene Symbol	FC E18.5 vs. E14.5			Muscle-related functions	Reference
		WT	$RYR1^{-/-}$	$Ca_v1.1^{-/-}$		
microRNA 376b	Mir376b	3.69	-	-	a role in cardioprotection	[51]
Other miRNAs implicated in skeletal muscle development						
RIKEN cDNA 6430411K18 gen; microRNA 127; microRNA 433	**6430411K18Rik**	**2.78**	-	-	**enhances myogenic cell differentiation**	[52]
microRNA 376a	**Mir376a**	**2.81**	-	-	**involved in skeletal muscle development**	[53]
microRNA 665	**Mir665**	**2.92**		**2.04**	**associated in secondary myogenesis in pigs**	[54]
microRNA 136	**Mir136**	**3.41**	-	-	**downregulated in mouse skeletal muscle after birth**	[41]
microRNA 434	**Mir434**	**3.55**	-	-	**influences AChRs expression in rat hind limb**	[55]
microRNA 540	**Mir540**	**3.56**	-	**2.05**	**induces hypertrophy in C2C12**	[56]
microRNA 432	Mir432	2.04	-	-	regulates myoblast proliferation and differentiation	[57]
microRNA 365–2	Mir365-2	2.04	-	-	putative inhibition of myogenic differentiation in C2C12	[58]
microRNA 145a	Mir145a	2.1	-	-	promotes myoblast differentiation	[59]
microRNA 22; Mir22 host gene (non-protein coding); TLC domain containing 2	Mir22	2.24	-	-	up-regulated during myocyte differentiation	[60]
microRNA 5123	Mir5123	2.29	-	-	upregulated in ageing muscle	[61]
miRNAs not yet described in skeletal muscle development						
microRNA 1193	**Mir1193**	**2.01**	-	-		
microRNA 329	**Mir329**	**2.15**	-	-		
microRNA 1188	**Mir1188**	**2.16**	-	-		
microRNA 543	**Mir543**	**2.43**	-	-		
retrotransposon-like 1; microRNA 3071	**Rtl1**	**3.54**	-	-		
microRNA 337	**Mir337**	**5.61**	-	**3.06**		
microRNA 882	Mir882	2.01	-	-		
microRNA 3070b	Mir3070b	2.81	-	2.01		
microRNA 3070a	Mir3070a	2.83	-	-		
microRNA 370	Mir370	3.02	-	-		
microRNA 493	Mir493	3.76	-	2.52		
microRNA 568; zinc finger and BTB domain containing 20	Mir568	4.41	2.65	-		
phosphodiesterase 4D interacting protein (myomegalin); microRNA 7225	Pde4dip	4.49	4.1	3.79		
miRNAs found exclusively in $RYR1^{-/-}$ skeletal muscle development (E18.5 vs. E14.5)						
microRNA 125b-1	Mir125b-1	-	-2.11	-		
miRNAs found exclusively in $Ca_v1.1^{-/-}$ skeletal muscle development (E18.5 vs. E14.5)						
microRNA 205; RIKEN cDNA 4631405K08 gene	Mir205	-	-	-2.38		
microRNA 669d	Mir669d	-	-	-2.07		
glutamate-ammonia ligase (glutamine synthetase); microRNA 8114	Glul	-	-	2.14		
microRNA 130a	Mir130a	-	-	2.28		

miRNAs reported as downregulated in ageing skeletal muscle are written in bold text [39]. The FCs of miRNAs not detected as differentially regulated in some of the conditions are marked as "-".

https://doi.org/10.1371/journal.pone.0194428.t003

characteristic signature [28]. The spectrum of severity resulting from mutations in RYR1 is demonstrated, for instance, in skeletal muscles from patients suffering from diseases like atypical periodic paralysis and myalgia [62], and by the lethal multiple pterygium syndrome [63].

Here we demonstrate that skeletal muscle from both homozygous $RYR1^{-/-}$ and $Ca_v1.1^{-/-}$ mice exhibits moderate but discrete morphological and transcriptomic changes already at E14.5, suggesting that RYR1 and $Ca_v1.1$ are involved in the embryonic development and primary myogenesis. Histological abnormalities and gene expression changes of these animals become much more overt at E18.5, demonstrating the vital importance of the two Ca^{2+} channels during fetal development of muscle. The latter term does not only refer to muscle cells or fibers in the narrower sense, but also comprises the other constituents of the muscle organ like nerves, blood vessels and connective tissue. As these structures take part in the normal development and the function of skeletal muscle, it is not only unavoidable but also desirable to have their transcriptomic impact integrated in the present analysis.

A first surprise in our analysis was to find that among the "early" DEGs, i.e. at E14.5, only 2 were shared by the homozygous mutants. Apart from these, the DEGs of $RYR1^{-/-}$ and $Ca_v1.1^{-/-}$ samples at this early stage were associated with different biological processes (Fig 9), suggesting that RYR1 and $Ca_v1.1$ have distinct roles during early myogenesis. E14.5 is approximately the stage at which the mouse embryos first begin to move [11]. Thus, although the cooperative action of both Ca^{2+} channels is required for proper ECC, they probably also exert additional, non-contractile functions during muscle development. At E14.5 the absence of RYR1 seems to negatively influence neuron differentiation and / or muscle innervation, whereas the lack of $Ca_v1.1$ is already linked to downregulation of genes involved in the muscle's contractile machinery. In cell culture, $Ca_v1.1$ is expressed prior RYR1 [64] where it has been shown to lead to activation of phospholipase C (PLC), leading to Ca^{2+} influx from the SR through the inositol 1,4,5-triphosphate receptor (IP3R) [65]. The IP3R-mediated Ca^{2+} transients have been implicated in myogenesis and in additional signaling paths [66,67], hence some of the $Ca_v1.1^{-/-}$ specific transcriptomic changes are probably caused by an impaired activation of IP3Rs. Alternatively (or additionally), the distinct transcriptomic changes in the mutants at E14.5 may also be connected to Ca^{2+} influx into the cells from the extracellular space through the embryonic (Δ29) $Ca_v1.1$ splice variant, which has been linked to acetylcholine receptor (AChR) pre-patterning of developing skeletal muscle [34]. We observed a higher ratio of Δ29 to full-length $Ca_v1.1$ mRNA in $RYR1^{-/-}$ compared to WT skeletal muscle at E14.5, which might be accompanied by an increased, $Ca_v1.1$-mediated Ca^{2+} influx into these muscles upon spontaneous or motor neuron-caused depolarization. At E18.5 the ratio of the Δ29 to full-length $Ca_v1.1$ mRNA was unchanged in $RYR1^{-/-}$ compared to WT samples, but the total $Ca_v1.1$ mRNA levels were decreased by 2-fold in the $RYR1^{-/-}$ samples, which is in line with previous reports [29,35,36]. In contrast, the complete absence of the dihydropyridine receptor in $Ca_v1.1^{-/-}$ muscle, with the consequence of absent voltage–dependent activation of RYR1 and IP3R, may explain the higher number of DEGs at both E14.5 and E18.5 in these mutants, as well as their more severe muscle phenotype. Interestingly, it has recently been demonstrated in a mouse model expressing exclusively a non-conducting $Ca_v1.1$, that the absence of $Ca_v1.1$-mediated Ca^{2+} influx does neither affect skeletal muscle development, contractile properties and contractile protein expression, nor the normal phenotype, fertility and longevity of these animals [68]. Taking these recent observations into account, the majority of morphological and transcriptomic alterations we find in our study in $Ca_v1.1^{-/-}$ limb skeletal muscle most likely are not the consequence of absent Ca^{2+} influx through $Ca_v1.1$, but would rather be caused by the lack of activation of RYR1- and/or IP3R-mediated Ca^{2+} release. Additionally, the physical absence of $Ca_v1.1$ as critical element for interactions within the macromolecular EC coupling apparatus could contribute to these deteriorations.

The serious alterations in skeletal muscle gross structure and histology of the mutants at E18.5 (as compared to E14.5; Fig 2) are in line with the 8 to 10-fold greater number of DEGs in $RYR1^{-/-}$ and $Ca_v1.1^{-/-}$ vs. WT at this later stage (Table 2). But not only the number of DEGs in both $RYR1^{-/-}$ and $Ca_v1.1^{-/-}$ is considerably greater at E18.5, there is also, in contrast to E14.5, a significant overlap in the identity of DEGs in both mutants. This indicates that the absence of mechanical movement and the lack of associated Ca^{2+} signaling lead to transcriptomic changes ultimately shared by both homozygous mice models, and probably also by developmental paralysis models in general (as discussed in [28]). Accordingly, at E18.5 multiple genes encoding proteins associated with the contractile machinery were downregulated in the mutants (Fig 10), possibly through a negative feedback loop due to the lack of mechanical loading. Some of these DEGs encode thick (*Myl2*, *Myh13*, *Myl9*, *Myh7*, *Myl6b*) and thin (*Tpm3*, *Myom1*, *Myom2*) filament proteins, Z-disc proteins (*Csrp3*, *Rcsd1*, *Actn2*, *Tcap*), as well as proteins taking part in the structure of costameres (*Myof*, *Ankrd2*, *Dmd*, *Sgca*, *Myot*) and ion channels (*Cacna1h*, *Kcne1l*, *Kcnma1*, *Ryr1*, *P2rx6*, *Cacna1s*, *Cacng1*, *Kcnq1*, *Clcn1*). These structures, especially the Z-disc and the costamere, play important roles in signal transmission between the ECM, the sarcolemma and the myofibrils, in the process of mechanotransduction [69,70]. Mechanical stimuli have been long known to contribute to muscle development and hypertrophy by activating an intricate network of downstream signaling cascades which include integrins, G-protein coupled receptors, the nuclear factor of activated T cells (NFAT), PI3K-Akt and MAPK pathways [15,71,72]. These signaling pathways are also regulated by changes in the cytosolic Ca^{2+} concentration which in turn is affected by various mechanosensitive pathways [16]. Thus, it is not surprising that the absence of RYR1 or $Ca_v1.1$ –each indispensable for the rapid Ca^{2+} release that triggers muscle contraction—causes changes in the expression of multiple genes, involved in these major signaling pathways (S4 Table).

Our study identified a higher number of DEGs for WT in the E18.5 vs. E14.5 comparison than for either mutant (Table 2). Thus, a considerable fraction of the DEGs found in the E18.5 mutants vs. WT comparison, might emerge from a failure in the two mutants to activate the normal developmental expression program. This is reflected by the processes associated with the DEGs emerging from the E18.5 vs. E14.5 comparison (Fig 12). Specifically, multiple genes involved in the cell cycle control (*Prim2*, *Ccnd2*, *Mcm7*, *Cdk4*, *Mcm2*, *Plk1*, *Mad2l1*) were downregulated only in WT samples—a typical sign for terminal differentiation. Moreover, many genes encoding proteins of the muscle contractile machinery were found to be upregulated from E14.5 to E18.5 exclusively in WTs (Fig 12F, S10 Table); or to be upregulated with a much smaller FC in the mutants like *Mybpc2*, *Ckmt2*, *Myh2*, *Myh4* and *Mylk2* (S1 Table). These observations strongly imply that the secondary myogenesis, normally involving an increased level and organization of contractile structures, and accompanied by the exit from the cell cycle during fetal development, is impaired in $RYR1^{-/-}$ and $Ca_v1.1^{-/-}$ limb skeletal muscle.

We have further detected a differential expression of at least 61 miRNAs in WT limb skeletal muscle from E14.5 to E18.5, with only a few of them undergoing a parallel regulation in both mutants (Table 3). Many miRNAs have been found to be potent regulators of gene expression in general and of muscle differentiation, in particular [73]. Therefore, the altered miRNA developmental patterns in $RYR1^{-/-}$ and $Ca_v1.1^{-/-}$ limb skeletal muscle are likely to have contributed to the observed transcriptomic changes. The vast majority of differentially expressed miRNAs identified in the WT showed an upregulation at E18.5 vs. E14.5. Interestingly, more than half of them were reported to be also downregulated in ageing skeletal muscle (Table 3) [39], suggesting important roles for these miRNAs in myogenesis and in skeletal muscle maintenance. In this respect, the *Dlk-Dio3* genomic region—a miRNA megacluster encoding more than 50 miRNAs—appears to be of eminent importance [74]: 26 of the

developmentally upregulated miRNAs we found in WT skeletal muscle originate from this region. Also, reduced expression of miRNAs from the *Dlk-Dio3* cluster has been implicated in the ageing process in gastrocnemius muscles [75], and myostatin deficiency has been shown to lead to a transcriptional activation of this locus [56]. Only 6 of the miRNAs upregulated in WT (E18.5 vs. E14.5) were also upregulated in $Ca_v1.1^{-/-}$ muscle and none in $RYR1^{-/-}$ muscle (Table 3). Thus, our findings indicate that the increased expression level of multiple miRNAs from the *Dlk-Dio3* genomic region is a significant contributor to secondary myogenesis and that muscle contraction probably drives their expression.

In the E18.5 vs. E14.5 comparison we observed sets of DEGs exclusively regulated in either $RYR1^{-/-}$ or $Ca_v1.1^{-/-}$ limb skeletal muscle (Fig 12). The cellular processes and structures affected by these DEGs in the $RYR1^{-/-}$ samples were related to bone, cartilage and neuron differentiation, focal adhesion and ion channels; whereas in the $Ca_v1.1^{-/-}$ samples these were predominantly processes linked to adipogenesis and lipid metabolism. Given the critical signaling role of $[Ca^{2+}]_i$, these differences may originate from the different resting $[Ca^{2+}]_i$ in both mutants—resting Ca^{2+} levels were found to be lower than in WT in cultured $RYR1^{-/-}$ myotubes and higher than in WT in $Ca_v1.1^{-/-}$ myotubes [76–78]. These results have been accounted for by a model in which $Ca_v1.1$ is necessary for inhibiting spontaneous Ca^{2+} leak trough RYR1. This model would also explain the upregulation of *Musk*, *Chrnd* and *Chrng*, detected only during development of $RYR1^{-/-}$ skeletal muscle, as these genes are negatively regulated by increased $[Ca^{2+}]_i$ and in turn regulate proper neuromuscular synaptic pre-patterning [79]. Additionally, as discussed above, the absence of $Ca_v1.1$ may also lead to explicit differences in gene expression because of lack or reduction of the IP3R-mediated Ca^{2+} transients. The evident changes in the expression of genes associated with lipid metabolism would also suggest alterations in mitochondrial function and / or mitochondrial Ca^{2+} uptake in $Ca_v1.1^{-/-}$ skeletal muscle. The latter could be a contributing factor to the increased levels of apoptosis observed in $Ca_v1.1^{-/-}$ skeletal muscle at E14.5, however, an increased lipotoxicity is also thinkable in this respect [80].

Unexpectedly, unlike the heterozygous $RYR1^{+/-}$ skeletal muscle, which does not display obvious alterations with respect to WT, heterozygous $Ca_v1.1^{+/-}$ skeletal muscle is characterized by morphological aberrations at both E14.5 and E18.5. Such a phenotype has not been reported previously for $Ca_v1.1^{+/-}$ skeletal muscle, which has been regarded as equivalent to WT [81–84]. Nevertheless, an altered mandible development has been described in $Ca_v1.1^{+/-}$ animals [85], indicating that a precise gene dosage of $Ca_v1.1$ may also be necessary for a stable muscle development. However, very few DEGs were detected between $Ca_v1.1^{+/-}$ and WT skeletal muscles at both E14.5 and E18.5 (Table 2).

Taken together, our findings provide important information about the changes occurring in the transcriptomic landscape of limb skeletal muscle during secondary myogenesis in mouse. We have shown that absence of RYR1 or $Ca_v1.1$ leads to partially severe histological changes in limb skeletal muscle both at the beginning (E14.5) and, more so, the end (E18.5) of secondary myogenesis. At both time points the global gene expression profiles of RYR1- and $Ca_v1.1$-deficient muscle exhibit significant changes, affecting an extensive array of genes related to structure and to key signaling pathways. At E14.5 we observed fewer but distinct DEGs in each mutant, whereas at E18.5 the expression changes in both mutants became vast and partially converged. The significantly higher number of affected genes at E18.5 together with the suppression of myogenic progression from E14.5 to E18.5 in both mutants, indicate that presence of RYR1 and $Ca_v1.1$ is essential during secondary myogenesis. Thus, we hypothesize that RYR1 and Cav1.1, beyond their critical role in skeletal muscle ECC, have also important, partially discrete roles in both embryonic and fetal skeletal muscle development. Future work will elucidate the molecular mechanisms by which RYR1 and $Ca_v1.1$ influence skeletal muscle development.

Supporting information

S1 Fig. $Ca_v1.1$ splice variants in WT and $RYR1^{-/-}$ skeletal muscle. Original photographs of agarose gels used for the analysis of PCR products of the full-length (343 bp) and Δ29 (286 bp) $Ca_v1.1$ splice variants in WT (A), and in $RYR1^{-/-}$ (B) animals at E14.5 (A and B, lanes 1–6) and E18.5 (A and B, lanes 8–13). (A and B) Lane 7—O'Gene Ruler Mix DNA ladder.
(TIF)

S2 Fig. RNA agarose gels. The integrity of the RNA samples used in the MA analyses was evaluated by subjecting 250 ng or 500 ng of each sample to electrophoretic runs on 2% agarose gels next to 2 μl of RiboRuler High Range RNA Ladder (Thermo Fisher Scientific). The genotypes of the mice are represented as follows: +/+ stands for WT, +/-—for heterozygous mutant and -/-—for homozygous mutant of the RYR1 and $Ca_v1.1$ lines, respectively. The numbers 1–3 represent the individual biological replicates (fetuses); "n." stands for samples that were not used in the MAs.
(TIF)

S3 Fig. qRT-PCR analyses of putative endogenous controls. The relative expression levels of *Gapdh*, *Actb*, *Rplp0*, *Uba52* and *CytB* (used as endogenous control) were measured via qRT-PCRs for WT E18.5 vs. E14.5 samples (A), as well as for $RYR1^{-/-}$ vs. WT (B and C) and for $Ca_v1.1^{-/-}$ vs. WT (D and E) at E14.5 and E18.5. Expression levels of control samples (blue bars) were set to 1. Statistical *t*-tests were performed for each gene, ***represents a p-value ≤ 0.001. Error bars are S.E.M.
(TIF)

S1 Table. All detected DEGs from the MAs from all performed comparisons.
(XLSX)

S2 Table. GO BP enrichment analyses of $RYR1^{-/-}$ or $Ca_v1.1^{-/-}$ vs. WT at E14.5.
(XLSX)

S3 Table. DEGs for heatmaps of $RYR1^{-/-}$ or $Ca_v1.1^{-/-}$ vs. WT at E14.5.
(XLSX)

S4 Table. DEGs in $RYR1^{-/-}$ or $Ca_v1.1^{-/-}$ vs. WT at E18.5 involved in signaling pathways.
(XLSX)

S5 Table. GO BP enrichment analyses of $RYR1^{-/-}$ or $Ca_v1.1^{-/-}$ vs. WT at E18.5.
(XLSX)

S6 Table. DEGs for "Muscle contraction" heatmap of $RYR1^{-/-}$ and $Ca_v1.1^{-/-}$ vs. WT at E18.5.
(XLSX)

S7 Table. DEGs for "Extracellular Matrix Organization" heatmap of $RYR1^{-/-}$ vs. WT at E18.5.
(XLSX)

S8 Table. DEGs for "Acylglycerol Metabolic Process" heatmap of $Ca_v1.1^{-/-}$ vs. WT at E18.5.
(XLSX)

S9 Table. GO BP and WP analyses of all DEGs in WT, $RYR1^{-/-}$ or $Ca_v1.1^{-/-}$ for E18.5 vs. E14.5.
(XLSX)

S10 Table. GO BP and WP analyses of unique DEGs in WT, $RYR1^{-/-}$ or $Ca_v1.1^{-/-}$ for E18.5 vs. E14.5.
(XLSX)

Acknowledgments

We thank Dr. Paul Allen (UC Davis) for creating, and Drs. Paul Allen and Vincenzo Sorrentino (University of Siena) for sharing, the *dyspedic* mouse model. We thank Drs. Robert Stehle, Mechthild Schroeter, Lubomir Lubomirov and Desirée Moehner for the valuable discussions.

Author Contributions

Conceptualization: Dilyana Filipova, Symeon Papadopoulos.

Data curation: Dilyana Filipova.

Formal analysis: Dilyana Filipova.

Funding acquisition: Symeon Papadopoulos.

Investigation: Dilyana Filipova, Margit Henry, Tamara Rotshteyn, Anna Brunn, Mariana Carstov, Symeon Papadopoulos.

Methodology: Dilyana Filipova, Anna Brunn, Symeon Papadopoulos.

Project administration: Dilyana Filipova, Symeon Papadopoulos.

Resources: Martina Deckert, Jürgen Hescheler, Agapios Sachinidis, Gabriele Pfitzer, Symeon Papadopoulos.

Supervision: Dilyana Filipova, Symeon Papadopoulos.

Visualization: Dilyana Filipova, Anna Brunn.

Writing – original draft: Dilyana Filipova, Anna Brunn, Symeon Papadopoulos.

Writing – review & editing: Dilyana Filipova, Margit Henry, Tamara Rotshteyn, Anna Brunn, Mariana Carstov, Martina Deckert, Jürgen Hescheler, Agapios Sachinidis, Gabriele Pfitzer, Symeon Papadopoulos.

References

1. Westerblad H, Bruton JD, Katz A (2010) Skeletal muscle: energy metabolism, fiber types, fatigue and adaptability. Exp Cell Res 316: 3093–3099. https://doi.org/10.1016/j.yexcr.2010.05.019 PMID: 20580710
2. Pedersen BK (2013) Muscle as a secretory organ. Compr Physiol 3: 1337–1362. https://doi.org/10.1002/cphy.c120033 PMID: 23897689
3. Eisenberg BR (2010) Quantitative Ultrastructure of Mammalian Skeletal Muscle. Comprehensive Physiology: John Wiley & Sons, Inc.
4. Deries M, Thorsteinsdottir S (2016) Axial and limb muscle development: dialogue with the neighbourhood. Cell Mol Life Sci 73: 4415–4431. https://doi.org/10.1007/s00018-016-2298-7 PMID: 27344602
5. Tajbakhsh S (2009) Skeletal muscle stem cells in developmental versus regenerative myogenesis. J Intern Med 266: 372–389. https://doi.org/10.1111/j.1365-2796.2009.02158.x PMID: 19765181
6. Biressi S, Molinaro M, Cossu G (2007) Cellular heterogeneity during vertebrate skeletal muscle development. Dev Biol 308: 281–293. https://doi.org/10.1016/j.ydbio.2007.06.006 PMID: 17612520
7. Duxson MJ, Usson Y, Harris AJ (1989) The origin of secondary myotubes in mammalian skeletal muscles: ultrastructural studies. Development 107: 743–750. PMID: 2483685

8. Evans D, Baillie H, Caswell A, Wigmore P (1994) During fetal muscle development, clones of cells contribute to both primary and secondary fibers. Dev Biol 162: 348–353. https://doi.org/10.1006/dbio.1994.1092 PMID: 8150199
9. Biressi S, Tagliafico E, Lamorte G, Monteverde S, Tenedini E, Roncaglia E, et al. (2007) Intrinsic phenotypic diversity of embryonic and fetal myoblasts is revealed by genome-wide gene expression analysis on purified cells. Dev Biol 304: 633–651. https://doi.org/10.1016/j.ydbio.2007.01.016 PMID: 17292343
10. Bentzinger CF, Wang YX, Rudnicki MA (2012) Building muscle: molecular regulation of myogenesis. Cold Spring Harb Perspect Biol 4.
11. Kodama N, Sekiguchi S (1984) The Development of Spontaneous Body Movement in Prenatal and Perinatal Mice. Developmental Psychobiology 17: 139–150. https://doi.org/10.1002/dev.420170205 PMID: 6706018
12. Sandow A (1952) Excitation-contraction coupling in muscular response. Yale J Biol Med 25: 176–201. PMID: 13015950
13. Szent-Gyorgyi AG (1975) Calcium regulation of muscle contraction. Biophys J 15: 707–723. https://doi.org/10.1016/S0006-3495(75)85849-8 PMID: 806311
14. Berchtold MW, Brinkmeier H, Muntener M (2000) Calcium ion in skeletal muscle: its crucial role for muscle function, plasticity, and disease. Physiol Rev 80: 1215–1265. https://doi.org/10.1152/physrev.2000.80.3.1215 PMID: 10893434
15. Gehlert S, Bloch W, Suhr F (2015) Ca2+-Dependent Regulations and Signaling in Skeletal Muscle: From Electro-Mechanical Coupling to Adaptation. Int J Mol Sci 16: 1066–1095. https://doi.org/10.3390/ijms16011066 PMID: 25569087
16. Benavides Damm T, Egli M (2014) Calcium's role in mechanotransduction during muscle development. Cell Physiol Biochem 33: 249–272. https://doi.org/10.1159/000356667 PMID: 24525559
17. Beam KG, Bannister RA (2010) Looking for answers to EC coupling's persistent questions. J Gen Physiol 136: 7–12. https://doi.org/10.1085/jgp.201010461 PMID: 20584887
18. Nakai J, Tanabe T, Konno T, Adams B, Beam KG (1998) Localization in the II-III loop of the dihydropyridine receptor of a sequence critical for excitation-contraction coupling. J Biol Chem 273: 24983–24986. PMID: 9737952
19. Papadopoulos S, Leuranguer V, Bannister RA, Beam KG (2004) Mapping sites of potential proximity between the dihydropyridine receptor and RyR1 in muscle using a cyan fluorescent protein-yellow fluorescent protein tandem as a fluorescence resonance energy transfer probe. J Biol Chem 279: 44046–44056. https://doi.org/10.1074/jbc.M405317200 PMID: 15280389
20. Polster A, Ohrtman JD, Beam KG, Papadopoulos S (2012) Fluorescence resonance energy transfer (FRET) indicates that association with the type I ryanodine receptor (RyR1) causes reorientation of multiple cytoplasmic domains of the dihydropyridine receptor (DHPR) alpha(1S) subunit. J Biol Chem 287: 41560–41568. https://doi.org/10.1074/jbc.M112.404194 PMID: 23071115
21. des Georges A, Clarke OB, Zalk R, Yuan Q, Condon KJ, Grassucci RA, et al. (2016) Structural Basis for Gating and Activation of RyR1. Cell 167: 145–157.e117. https://doi.org/10.1016/j.cell.2016.08.075 PMID: 27662087
22. Cannon SC (2015) Channelopathies of skeletal muscle excitability. Compr Physiol 5: 761–790. https://doi.org/10.1002/cphy.c140062 PMID: 25880512
23. Casey J, Flood K, Ennis S, Doyle E, Farrell M, Lynch SA (2016) Intra-familial variability associated with recessive RYR1 mutation diagnosed prenatally by exome sequencing. Prenat Diagn 36: 1020–1026. https://doi.org/10.1002/pd.4925 PMID: 27616680
24. Takeshima H, Iino M, Takekura H, Nishi M, Kuno J, Minowa O, et al. (1994) Excitation-contraction uncoupling and muscular degeneration in mice lacking functional skeletal muscle ryanodine-receptor gene. Nature 369: 556–559. https://doi.org/10.1038/369556a0 PMID: 7515481
25. Franzini-Armstrong C, Pincon-Raymond M, Rieger F (1991) Muscle fibers from dysgenic mouse in vivo lack a surface component of peripheral couplings. Dev Biol 146: 364–376. PMID: 1650725
26. Pai AC (1965) Developmental Genetics of a Lethal Mutation, Muscular Dysgenesis (Mdg), in the Mouse. I. Genetic Analysis and Gross Morphology. Dev Biol 11: 82–92. PMID: 14300095
27. Pai AC (1965) Developmental Genetics of a Lethal Mutation, Muscular Dysgenesis (Mdg), in the Mouse. Ii. Developmental Analysis. Dev Biol 11: 93–109. PMID: 14300096
28. Filipova D, Walter AM, Gaspar JA, Brunn A, Linde NF, Ardestani MA, et al. (2016) Gene profiling of embryonic skeletal muscle lacking type I ryanodine receptor Ca(2+) release channel. Sci Rep 6: 20050. https://doi.org/10.1038/srep20050 PMID: 26831464
29. Buck ED, Nguyen HT, Pessah IN, Allen PD (1997) Dyspedic mouse skeletal muscle expresses major elements of the triadic junction but lacks detectable ryanodine receptor protein and function. J Biol Chem 272: 7360–7367. PMID: 9054435

30. Ye J, Coulouris G, Zaretskaya I, Cutcutache I, Rozen S, Madden TL (2012) Primer-BLAST: a tool to design target-specific primers for polymerase chain reaction. BMC Bioinformatics 13: 134. https://doi.org/10.1186/1471-2105-13-134 PMID: 22708584

31. Chen EY, Tan CM, Kou Y, Duan Q, Wang Z, Meirelles GV, et al. (2013) Enrichr: interactive and collaborative HTML5 gene list enrichment analysis tool. BMC Bioinformatics 14: 128. https://doi.org/10.1186/1471-2105-14-128 PMID: 23586463

32. Metsalu T, Vilo J (2015) ClustVis: a web tool for visualizing clustering of multivariate data using Principal Component Analysis and heatmap. Nucleic Acids Res 43: W566–570. https://doi.org/10.1093/nar/gkv468 PMID: 25969447

33. Tuluc P, Molenda N, Schlick B, Obermair GJ, Flucher BE, Jurkat-Rott K (2009) A CaV1.1 Ca2+ channel splice variant with high conductance and voltage-sensitivity alters EC coupling in developing skeletal muscle. Biophys J 96: 35–44. https://doi.org/10.1016/j.bpj.2008.09.027 PMID: 19134469

34. Flucher BE, Tuluc P (2011) A new L-type calcium channel isoform required for normal patterning of the developing neuromuscular junction. Channels (Austin) 5: 518–524.

35. Nakai J, Dirksen RT, Nguyen HT, Pessah IN, Beam KG, Allen PD (1996) Enhanced dihydropyridine receptor channel activity in the presence of ryanodine receptor. Nature 380: 72–75. https://doi.org/10.1038/380072a0 PMID: 8598910

36. Avila G, O'Connell KM, Groom LA, Dirksen RT (2001) Ca2+ release through ryanodine receptors regulates skeletal muscle L-type Ca2+ channel expression. J Biol Chem 276: 17732–17738. https://doi.org/10.1074/jbc.M009685200 PMID: 11278546

37. Luo W, Nie Q, Zhang X (2013) MicroRNAs involved in skeletal muscle differentiation. J Genet Genomics 40: 107–116. https://doi.org/10.1016/j.jgg.2013.02.002 PMID: 23522383

38. Chen JF, Mandel EM, Thomson JM, Wu Q, Callis TE, Hammond SM, et al. (2006) The role of microRNA-1 and microRNA-133 in skeletal muscle proliferation and differentiation. Nat Genet 38: 228–233. https://doi.org/10.1038/ng1725 PMID: 16380711

39. Lee KP, Shin YJ, Panda AC, Abdelmohsen K, Kim JY, Lee SM, et al. (2015) miR-431 promotes differentiation and regeneration of old skeletal muscle by targeting Smad4. Genes Dev 29: 1605–1617. https://doi.org/10.1101/gad.263574.115 PMID: 26215566

40. Qin Y, Peng Y, Zhao W, Pan J, Ksiezak-Reding H, Cardozo C, et al. (2017) Myostatin inhibits osteoblastic differentiation by suppressing osteocyte-derived exosomal microRNA-218: A novel mechanism in muscle-bone communication. J Biol Chem 292: 11021–11033. https://doi.org/10.1074/jbc.M116.770941 PMID: 28465350

41. Lamon S, Zacharewicz E, Butchart LC, Orellana L, Mikovic J, Grounds MD, et al. (2017) MicroRNA expression patterns in post-natal mouse skeletal muscle development. BMC Genomics 18: 52. https://doi.org/10.1186/s12864-016-3399-2 PMID: 28061746

42. Fiorillo AA, Heier CR, Novak JS, Tully CB, Brown KJ, Uaesoontrachoon K, et al. (2015) TNF-alpha-Induced microRNAs Control Dystrophin Expression in Becker Muscular Dystrophy. Cell Rep 12: 1678–1690. https://doi.org/10.1016/j.celrep.2015.07.066 PMID: 26321630

43. Jeanson-Leh L, Lameth J, Krimi S, Buisset J, Amor F, Le Guiner C, et al. (2014) Serum profiling identifies novel muscle miRNA and cardiomyopathy-related miRNA biomarkers in Golden Retriever muscular dystrophy dogs and Duchenne muscular dystrophy patients. Am J Pathol 184: 2885–2898. https://doi.org/10.1016/j.ajpath.2014.07.021 PMID: 25194663

44. Forterre A, Jalabert A, Chikh K, Pesenti S, Euthine V, Granjon A, et al. (2014) Myotube-derived exosomal miRNAs downregulate Sirtuin1 in myoblasts during muscle cell differentiation. Cell Cycle 13: 78–89. https://doi.org/10.4161/cc.26808 PMID: 24196440

45. Katase N, Terada K, Suzuki T, Nishimatsu S, Nohno T (2015) miR-487b, miR-3963 and miR-6412 delay myogenic differentiation in mouse myoblast-derived C2C12 cells. BMC Cell Biol 16: 13. https://doi.org/10.1186/s12860-015-0061-9 PMID: 25925429

46. Wu R, Li H, Zhai L, Zou X, Meng J, Zhong R, et al. (2015) MicroRNA-431 accelerates muscle regeneration and ameliorates muscular dystrophy by targeting Pax7 in mice. Nat Commun 6: 7713. https://doi.org/10.1038/ncomms8713 PMID: 26151913

47. Eisenberg I, Eran A, Nishino I, Moggio M, Lamperti C, Amato AA, et al. (2007) Distinctive patterns of microRNA expression in primary muscular disorders. Proc Natl Acad Sci U S A 104: 17016–17021. https://doi.org/10.1073/pnas.0708115104 PMID: 17942673

48. Harafuji N, Schneiderat P, Walter MC, Chen YW (2013) miR-411 is up-regulated in FSHD myoblasts and suppresses myogenic factors. Orphanet J Rare Dis 8: 55. https://doi.org/10.1186/1750-1172-8-55 PMID: 23561550

49. Sun M, Huang F, Yu D, Zhang Y, Xu H, Zhang L, et al. (2015) Autoregulatory loop between TGF-beta1/miR-411-5p/SPRY4 and MAPK pathway in rhabdomyosarcoma modulates proliferation and differentiation. Cell Death Dis 6: e1859. https://doi.org/10.1038/cddis.2015.225 PMID: 26291313

50. Meyer SU, Thirion C, Polesskaya A, Bauersachs S, Kaiser S, Krause S, et al. (2015) TNF-alpha and IGF1 modify the microRNA signature in skeletal muscle cell differentiation. Cell Commun Signal 13: 4. https://doi.org/10.1186/s12964-015-0083-0 PMID: 25630602

51. Pan Z, Guo Y, Qi H, Fan K, Wang S, Zhao H, et al. (2012) M3 subtype of muscarinic acetylcholine receptor promotes cardioprotection via the suppression of miR-376b-5p. PLoS One 7: e32571. https://doi.org/10.1371/journal.pone.0032571 PMID: 22396777

52. Zhai L, Wu R, Han W, Zhang Y, Zhu D (2017) miR-127 enhances myogenic cell differentiation by targeting S1PR3. Cell Death Dis 8: e2707. https://doi.org/10.1038/cddis.2017.128 PMID: 28358363

53. McDaneld TG, Smith TP, Doumit ME, Miles JR, Coutinho LL, Sonstegard TS, et al. (2009) MicroRNA transcriptome profiles during swine skeletal muscle development. BMC Genomics 10: 77. https://doi.org/10.1186/1471-2164-10-77 PMID: 19208255

54. Verardo LL, Nascimento CS, Silva FF, Gasparino E, Toriyama E, Barbosa AR, et al. (2013) Identification and expression levels of pig miRNAs in skeletal muscle. Livestock Science 154: 45–54.

55. Shang FF, Xia QJ, Liu W, Xia L, Qian BJ, You L, et al. (2016) miR-434-3p and DNA hypomethylation co-regulate eIF5A1 to increase AChRs and to improve plasticity in SCT rat skeletal muscle. Scientific Reports 6.

56. Hitachi K, Tsuchida K (2017) Myostatin-deficiency in mice increases global gene expression at the Dlk1-Dio3 locus in the skeletal muscle. Oncotarget 8: 5943–5953. https://doi.org/10.18632/oncotarget.13966 PMID: 27992376

57. Ren RM, Liu H, Zhao SH, Cao JH (2016) Targeting of miR-432 to myozenin1 to regulate myoblast proliferation and differentiation. Genet Mol Res 15.

58. Sun L, Xie HM, Mori MA, Alexander R, Yuan BB, Hattangadi SM, et al. (2011) Mir193b-365 is essential for brown fat differentiation. Nature Cell Biology 13: 958–U198. https://doi.org/10.1038/ncb2286 PMID: 21743466

59. Du JJ, Li Q, Shen LY, Lei HG, Luo J, Liu YH, et al. (2016) miR-145a-5p Promotes Myoblast Differentiation. Biomed Research International.

60. Huang ZP, Chen J, Seok HY, Zhang Z, Kataoka M, Hu X, et al. (2013) MicroRNA-22 regulates cardiac hypertrophy and remodeling in response to stress. Circ Res 112: 1234–1243. https://doi.org/10.1161/CIRCRESAHA.112.300682 PMID: 23524588

61. Soriano-Arroquia A, House L, Tregilgas L, Canty-Laird E, Goljanek-Whysall K (2016) The functional consequences of age-related changes in microRNA expression in skeletal muscle. Biogerontology 17: 641–654. https://doi.org/10.1007/s10522-016-9638-8 PMID: 26922183

62. Matthews E, Neuwirth C, Jaffer F, Scalco RS, Fialho D, Parton M, et al. (2018) Atypical periodic paralysis and myalgia: A novel RYR1 phenotype. Neurology.

63. McKie AB, Alsaedi A, Vogt J, Stuurman KE, Weiss MM, Shakeel H, et al. (2014) Germline mutations in RYR1 are associated with foetal akinesia deformation sequence/lethal multiple pterygium syndrome. Acta Neuropathol Commun 2: 148. https://doi.org/10.1186/s40478-014-0148-0 PMID: 25476234

64. Kyselovic J, Leddy JJ, Ray A, Wigle J, Tuana BS (1994) Temporal differences in the induction of dihydropyridine receptor subunits and ryanodine receptors during skeletal muscle development. J Biol Chem 269: 21770–21777. PMID: 8063821

65. Eltit JM, Garcia AA, Hidalgo J, Liberona JL, Chiong M, Lavandero S, et al. (2006) Membrane electrical activity elicits inositol 1,4,5-trisphosphate-dependent slow Ca2+ signals through a Gbetagamma/phosphatidylinositol 3-kinase gamma pathway in skeletal myotubes. J Biol Chem 281: 12143–12154. https://doi.org/10.1074/jbc.M511218200 PMID: 16513646

66. Carrasco MA, Riveros N, Rios J, Muller M, Torres F, Pineda J, et al. (2003) Depolarization-induced slow calcium transients activate early genes in skeletal muscle cells. Am J Physiol Cell Physiol 284: C1438–1447. https://doi.org/10.1152/ajpcell.00117.2002 PMID: 12529240

67. Juretic N, Urzua U, Munroe DJ, Jaimovich E, Riveros N (2007) Differential gene expression in skeletal muscle cells after membrane depolarization. J Cell Physiol 210: 819–830. https://doi.org/10.1002/jcp.20902 PMID: 17146758

68. Dayal A, Schrotter K, Pan Y, Fohr K, Melzer W, Grabner M (2017) The Ca(2+) influx through the mammalian skeletal muscle dihydropyridine receptor is irrelevant for muscle performance. Nat Commun 8: 475. https://doi.org/10.1038/s41467-017-00629-x PMID: 28883413

69. Frank D, Kuhn C, Katus HA, Frey N (2006) The sarcomeric Z-disc: a nodal point in signalling and disease. J Mol Med (Berl) 84: 446–468.

70. Danowski BA, Imanaka-Yoshida K, Sanger JM, Sanger JW (1992) Costameres are sites of force transmission to the substratum in adult rat cardiomyocytes. J Cell Biol 118: 1411–1420. PMID: 1522115

71. Yamada AK, Verlengia R, Bueno CR Junior (2012) Mechanotransduction pathways in skeletal muscle hypertrophy. J Recept Signal Transduct Res 32: 42–44. https://doi.org/10.3109/10799893.2011.641978 PMID: 22171534

72. Tidball JG (2005) Mechanical signal transduction in skeletal muscle growth and adaptation. Journal of Applied Physiology 98: 1900–1908. https://doi.org/10.1152/japplphysiol.01178.2004 PMID: 15829723

73. Goljanek-Whysall K, Sweetman D, Munsterberg AE (2012) microRNAs in skeletal muscle differentiation and disease. Clin Sci (Lond) 123: 611–625.

74. Glazov EA, McWilliam S, Barris WC, Dalrymple BP (2008) Origin, evolution, and biological role of miRNA cluster in DLK-DIO3 genomic region in placental mammals. Mol Biol Evol 25: 939–948. https://doi.org/10.1093/molbev/msn045 PMID: 18281269

75. Kim JY, Park YK, Lee KP, Lee SM, Kang TW, Kim HJ, et al. (2014) Genome-wide profiling of the microRNA-mRNA regulatory network in skeletal muscle with aging. Aging (Albany NY) 6: 524–544.

76. Avila G, O'Brien JJ, Dirksen RT (2001) Excitation—contraction uncoupling by a human central core disease mutation in the ryanodine receptor. Proc Natl Acad Sci U S A 98: 4215–4220. https://doi.org/10.1073/pnas.071048198 PMID: 11274444

77. Eltit JM, Yang T, Li H, Molinski TF, Pessah IN, Allen PD, et al. (2010) RyR1-mediated Ca2+ leak and Ca2+ entry determine resting intracellular Ca2+ in skeletal myotubes. J Biol Chem 285: 13781–13787. https://doi.org/10.1074/jbc.M110.107300 PMID: 20207743

78. Eltit JM, Li H, Ward CW, Molinski T, Pessah IN, Allen PD, et al. (2011) Orthograde dihydropyridine receptor signal regulates ryanodine receptor passive leak. Proc Natl Acad Sci U S A 108: 7046–7051. https://doi.org/10.1073/pnas.1018380108 PMID: 21482776

79. Chen F, Liu Y, Sugiura Y, Allen PD, Gregg RG, Lin W (2011) Neuromuscular synaptic patterning requires the function of skeletal muscle dihydropyridine receptors. Nat Neurosci 14: 570–577. https://doi.org/10.1038/nn.2792 PMID: 21441923

80. Akhmedov D, Berdeaux R (2013) The effects of obesity on skeletal muscle regeneration. Front Physiol 4: 371. https://doi.org/10.3389/fphys.2013.00371 PMID: 24381559

81. Herring SW, Lakars TC (1982) Craniofacial development in the absence of muscle contraction. J Craniofac Genet Dev Biol 1: 341–357. PMID: 7119092

82. Flucher BE, Andrews SB, Fleischer S, Marks AR, Caswell A, Powell JA (1993) Triad formation: organization and function of the sarcoplasmic reticulum calcium release channel and triadin in normal and dysgenic muscle in vitro. J Cell Biol 123: 1161–1174. PMID: 8245124

83. Chaudhari N, Beam KG (1989) The Muscular Dysgenesis Mutation in Mice Leads to Arrest of the Genetic Program for Muscle Differentiation. Developmental Biology 133: 456–467. PMID: 2731637

84. Bannister RA, Papadopoulos S, Haarmann CS, Beam KG (2009) Effects of inserting fluorescent proteins into the alpha1S II-III loop: insights into excitation-contraction coupling. J Gen Physiol 134: 35–51. https://doi.org/10.1085/jgp.200910241 PMID: 19564426

85. Atchley WR, Herring SW, Riska B, Plummer AA (1984) Effects of the Muscular Dysgenesis Gene on Developmental Stability in the Mouse Mandible. Journal of Craniofacial Genetics and Developmental Biology 4: 179–189. PMID: 6501560